A NUMERICAL PARAMETRIC STUDY ON THE INFLUENCE OF THE BOND PATTERN ON THE TWO-WAY OUT-OF-PLANE BENDING CAPACITY OF MASONRY WALLS

MASTER THESIS

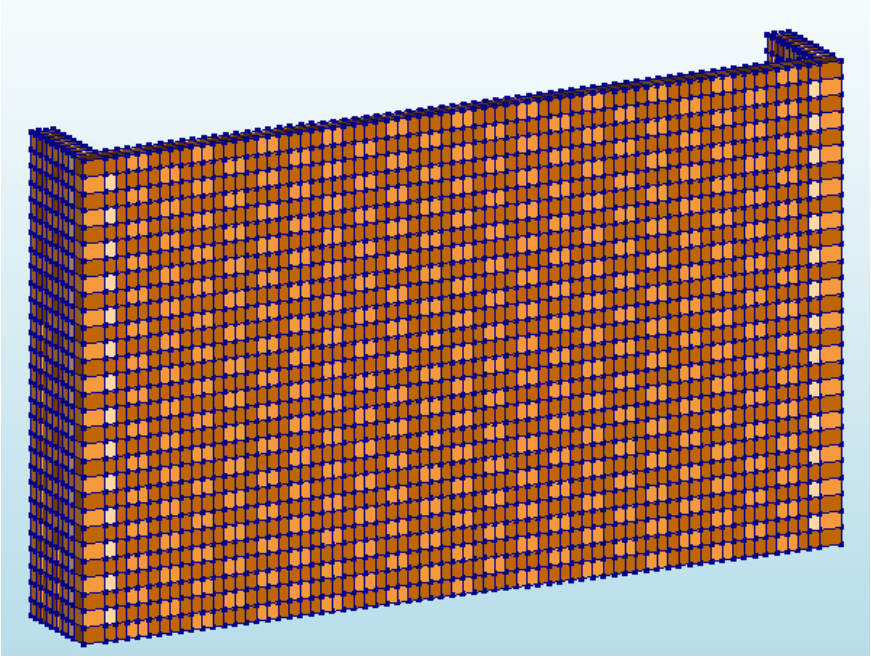

Stefan Niels Martijn ALBLAS

TU Delft Delft University of Technology

A NUMERICAL PARAMETRIC STUDY ON THE INFLUENCE OF THE BOND PATTERN ON THE TWO-WAY OUT-OF-PLANE BENDING CAPACITY OF MASONRY WALLS

MASTER THESIS
by

Stefan Niels Martijn ALBLAS

as a part of the degree of

Master of Science in
Civil Engineering

at Delft University of Technology,
to be defended publicly on Wednesday July 31, 2024 at 13:00

Thesis commitee:

Dr. R. Esposito (chair)	TU Delft Structural Mechanics
Dr. F. Messali	TU Delft Structural Mechanics
Ir. S. Pasterkamp	TU Delft Structural Design

PREFACE

I have studied for 8 years at TU Delft University of Technology. First, I completed my bachelor and immediately afterwards started on my Masters. This thesis is the conclusion of the Master Civil Engineering - Concrete Structures.

I want to especially thank the chair of my thesis committee, dr. Rita Esposito. She helped me enormously by her guidance and questions. Additionally, I also want to thank the members of my thesis committee; dr. Francesco Messali and ir. Sander Pasterkamp for their expertise and help during our meetings.

Finally, the support from my friends during my education has been highly appreciated. The support of my parents, my brother and my grandparents has been endless, and I would not have succeeded without them.

Stefan Niels Martijn Alblas
July 2024, Pijnacker

ABSTRACT

Masonry structures subjected to a lateral load, such as earthquakes and wind, can be prone to out-of-plane failure. It is known that geometrical properties and boundary conditions have a large influence on the out-of-plane bending capacity of walls. Nevertheless, limited information is available regarding the effect of bond pattern, in particular regarding the response of two-way spanning walls.
In this thesis, a numerical study is performed to evaluate the influence of the bond pattern on the two-way out-of-plane bending capacity of unreinforced brick masonry walls. A nonlinear finite element analysis with a 3D block-based model has been adopted to simulate the texture of the wall in detail. The study builds on the work of Chang et al. [1, 2], which was validated against the experimental benchmarks by Griffith et al. [3]. The numerical model can accurately estimate the initial stiffness and out-of-plane bending capacity, but the model is less accurate post-peak. Bricks are modelled with solid elements, while zero-thickness interface elements are used for the mortar joints. For the bricks, a rotating smeared cracking model considering an exponential tensile softening and an elastic response in compression was considered. For the mortar joints, the combined cracking-crushing-shear interface model was considered with an exponential softening in tension and shear and a parabolic curve in compression. It is assumed that the material properties of the mortar in the bed joints are the same as the one of the head and collar joints. The masonry wall was first subjected to self-weight and a vertical pre-compression of 0.1 MPa. Afterwards, a monotonic out-of-plane pressure placed on the face of the masonry wall is applied. The numerical model takes both physical and geometrical nonlinearity into account.
In the first phase, different modelling assumptions were checked and a sensitivity study was performed. Prior to the study must the compressive behaviour of the brick be determined, as the bricks are elastic without a limit, thus nonlinear effects like crushing are not modelled. The compressive stresses within the bricks in the entire model have been examined and the minimum principal stress does not exceed the compressive strength of the brick. The lowest minimum principal stress occurs post-peak of the two-way out-of-plane bending capacity and is not an issue. A mesh sensitivity study has also been performed as a change in mesh size was needed. In the model of Chang [1, 2], the face of the brick was divided over its length into two parts called a halfbrick (Hbrick). The stretcher bond can be implemented in a mesh size this large, however, other bond patterns require a division of the face into 4 parts, a quarterbrick (Qbrick). An even smaller mesh size which maintains the aspect ratio of the Hbrick by halving the Qbrick along its height was also tested, an octogonalbrick (Obrick). After the sensitivity study, it was determined that the Qbrick mesh is the best option, as the results of the three meshes are identical while the Obrick has become too complex as convergence issues arose. The influence of the cracking model within the bricks has also been analysed. In the numerical model a smeared cracking model within the brick is used, which smears the crack out

over the brick elements. Experiments have shown that cracks can propagate through the bricks. To simulate this effect a discrete cracking model within the brick was introduced instead of the smeared cracking model. The discrete cracking model requires the user to choose the locations for the cracks. The possible locations of the cracks can easily be assumed in a masonry wall, to be in line with a mortar joint in the course above or below it. The change to the discrete cracking model did not influence the out-of-plane two-way bending capacity, while convergence issues arose, and it was subsequently not used. The final assumption to be checked before the research into the bond patterns was the lateral boundary condition. In the experiment by Griffith et al. [3], clamps are installed over the height of the end of the return walls. These clamps prevent any horizontal translations and rotations in the horizontal plane. These clamps are represented by tyings in the numerical model and these are straight lines stretching from the bottom course to the top course situated at the edges of the end of the return walls. The bottom of the line is connected to the mortar joint between the bottom course and the vertical support. The tyings equalise both horizontal translations for all nodes on the line and as such the end of the return wall moves as one piece. All horizontal movement is prevented as the tyings are connected to the support. The location of the tyings ensures no rotation. The model with tyings achieves a higher out-of-plane bending capacity by restricting the boundary conditions which forces two-way bending. A masonry wall without any return walls is fully one-way bending and to the length of the return wall of 360 mm long does the masonry wall show a transition between one-way to two-way bending. A return wall of at least 480 mm long is sufficiently long to achieve two-way bending.
A parametric study was performed considering five single wythe and three double wythe bond patterns: stretcher bond, quarter bat bond, lateral bond, half Flemish bond, stack bond, chain bond, English bond and Flemish bond. The double wythe masonry wall has been assembled by adding an outer shell to the single wythe wall and by decreasing the pre-compression to 0.0478 MPa to maintain the same vertical force as the single wythe bonds. This does influence the out-of-plane bending capacity as an increase in the pre-compression results in a higher out-of-plane bending capacity as shown in experiments by Griffith et al. [3].
The highest out-of-plane bending capacity for the single wythe bond patterns is the half Flemish bond with 4.9 kPa and for the double wythe bond patterns it is the Flemish bond with 18.7 kPa. The differences between the highest and lowest bending capacity are 5.4% and 7.2%, respectively. The spread between the highest and lowest out-of-plane bending capacity is small. All the walls, except the one in stacked bonded masonry, show a crack pattern in the form of a cross made of four diagonal cracks starting approximately from the corners of the wall and one horizontal crack at the centre of the wall. The slopes of the diagonal cracks with respect to the horizontal bed joint line have also been studied and relates to the two-way bending capacity. A shallow slope in the crack pattern coincides with a higher two-way out-of-plane bending capacity. While a steeper slope or the absence of a cross-shaped pattern coincides with a lower out-of-plane bending capacity. On the contrary, the initial stiffness of the masonry wall does not relate to the out-of-plane bending capacity. To further confirm these findings, research is needed concerning different masonry types, considering relative properties between bricks and mortar joints, different properties between bed, head and collar joints, and spatial variability of properties.

CONTENTS

1

INTRODUCTION

Masonry structures have been built since antiquity. Over two thousand years ago, the Romans already built masonry structures. Figure 1.1 depicts the masonry of one such structure in the Roman city of Pompeii. Which was buried after an eruption of Mount Vesuvius in AD 79 and has since remained untouched. Sometimes a bond pattern is present there, as can be seen in the lower parts of the structure depicted in the figure. Higher up in the structure, bricks were just laid to ensure no vertical joint stretches through two courses: no particular bonding pattern was used. These masonry walls were built for vertical loads but have withstood the lateral load from earthquakes, ash and lava very well.

A failure mode for a masonry wall under lateral loading is out-of-plane failure. The resistance to lateral loading is provided by deformation of the masonry wall. This deformation of the masonry wall materialises in one-way and two-way bending. One-way bending is the bending around one axis while two-way bending is around two. The bond pattern that is used when building masonry structures might have a significant effect on the two-way out-of-plane bending capacity. Other examples of masonry walls under horizontal area load are quay walls and walls hit by earthquakes, which are becoming a more frequent occurrence in the Netherlands. The masonry structures for a quay wall are often built using multiple wythes to be strong enough to hold back water. The two-way out-of-plane bending capacity of masonry walls has been determined in multiple experiments. However, these experiments all had other primary goals. The effect of openings within the masonry wall was studied in BCRA (1977-1986), Chen (2002), Chong (1993), Griffith and Vaculik (2007), Ravenhorst et al. (2016), Tapp and Southcombe (1985, 1988), Vaculik et al. (2012, 2018) and Vekey et al. (1996). The other main parameter studied was the effect of the aspect ratio of a masonry wall, in BRCA (1977-1986), Chong (1993), Derakhshan et al. (2018), Griffith and Vaculik (2007) and Tapp and Southcombe (1985, 1988). These are a lot of studies on masonry walls, but in all this literature, only one experiment performs a numerical study. The numerical study was done by Chang et al. [1, 2] and analysed both the aspect ratio and the effect of an opening. Only two studies, namely those by Messali et al. (2017) and Padalu et al. (2020) include a sample using a bond pattern other than

the stretcher bond. The other bond pattern used is the English bond which is also a bond pattern with a double wythe. Now that the gap in current research is identified, can the scope of this thesis be determined:

The main research question is:

What is the effect of the bonding pattern on the two-way out-of-plane bending capacity of a masonry wall?

With the sub-questions:

1. Which geometric parameters influence the two-way out-of-plane bending capacity of a masonry wall?
2. What is the effect of the bond pattern on the two-way out-of-plane bending capacity of single wythe masonry walls?
3. What is the effect of a masonry wall's thickness on the two-way out-of-plane bending capacity?

This thesis studies the effect of the bond pattern on the two-way out-of-plane bending capacity of unreinforced masonry (URM) walls using a numerical computational model. The model, developed by Chang and used in Chang et al. (2021, 2022) [1, 2], is adapted and an additional validation is performed. The numerical model can only be used if the compressive behaviour of the bricks is verified. The bricks are assumed to be elastic in compression without a limit to the compressive strength of the brick. The computational model does not incorporate the nonlinear effect of crushing. A mesh sensitivity study is performed to check the significance of the mesh size. In the numerical model by Chang [1, 2], the face of the brick is divided over its length into two parts, called a halfbrick (Hbrick). This mesh size is too large for the other bond patterns which need at least a division of the face into four parts. Two mesh sizes are compared to the Hbrick and analysed, the quarterbrick (Qbrick) and octogonalbrick (Obrick). The effect of the cracking model will also be determined, since both a discrete and a smeared crack model can be used. In the numerical model is a smeared cracking model used, however, experiments by Griffith et al. [3] and Padalu et al. [4] have shown that bricks can crack vertically in line with the mortar joints of the courses above and below. The discrete cracking model is used to simulate these vertical cracks within the bricks. Other than the cracking model, the length of the return wall and its boundary conditions also influence the out-of-plane bending capacity. In the experimental campaign by Griffith et al. [3] return walls are clamped and restrained along the height at their end. The effect of the length of the return wall on the out-of-plane bending capacity is also determined in this study.

The effect of the bond patterns is then researched using load-displacement curves and the crack patterns. The results are cross-referenced to the experimental results by Griffith et al. [3] and Padalu et al. [4]. Five single wythe and three double wythe bond patterns are considered in this study, namely the stretcher bond, lateral bond, quarter bat bond, half Flemish bond, stack bond, chain bond, English bond, and Flemish bond. These bond patterns are compared to the bond patterns that share the same wythe, but an overall comparison between all bond patterns is also discussed.

Figure 1.1: Masonry used in a building in the city of Pompeii, the structure was buried after an eruption of Mount Vesuvius in AD 79

This thesis starts with previous research conducted using experimental testing campaigns and highlights the goal of these studies. Subsequently, four modelling strategies for out-of-plane loaded structures are mentioned and especially a Block-Based model (BBM) is discussed. Chapter 3 discusses the model designed by Chang and the modifications to his model to accommodate the numerical model to the multiple different bond patterns. The changes to the numerical model are validated in chapter 4. Chapter 5 concerns the analysis of the out-of-plane bending capacity and crack pattern of the bond patterns and chapter 6 describes the conclusion and offers recommendations for future work.

2

LITERATURE REVIEW

2.1. EXPERIMENTAL TESTING CAMPAIGNS

There have been many testing campaigns in the last 50 years. An overview of these testing campaigns is shown in table 2.1, including important parameters. These parameters comprise the numerical parametric studies performed with the experimental data, number of samples, presence of openings within the wall, multiple aspect ratios, bond patterns and the number of wythes. The number of samples in a testing campaign varied, in total 104 masonry walls were tested. These masonry wall samples were divided across fifteen testing campaigns. Nine of these campaigns consisted for 50% of walls which contained an opening and five of them compared aspect ratios. This shows that some important parameters to the out-of-plane bending capacity have been studied extensively. On the contrary, the bonding pattern has only been studied twice with a single sample. What is more, these two occasions are the only instances where the wythe has been changed. Additionally, a numerical parametric study has only been performed once. The effect of the bond pattern as well as the effect of the wythe have thus not been studied. While numerical parametric analyses have not been performed often, they could offer a valuable supplement to extensive practical experiments. Chang [2] has shown that a numerical model is a useful and accurate way to simulate a masonry wall. Some modelling strategies for structures and specifically masonry walls are discussed in the next chapter.

Table 2.1: Study of physical experiments, summarized from Chang [2, 5]

Testing campaign	Numeric parametric study performed	Number of samples	Samples with openings present	Number of aspect ratios	Bond pattern	Variable number of wythes
BCRA (1977-1986) [6]	No	16	15	3	Stretcher: 16	No
Chen (2002) [7]	No	8	7	1	Stretcher: 8	No
Chong (1993) [8]	No	16	11	2	Stretcher: 16	No
Derakhshan et al. (2018) [9]	No	3	0	3	Stretcher: 3	No
Grazotti et al. (2019) [10]	No	4	1	1	Stretcher: 4	No
Griffith and Vaculik (2007) [3]	Yes [1, 2]	8	6	2	Stretcher: 8	No
Messali et al. (2017) [11]	No	5	1	1	Stretcher: 4 English: 1	Yes
Padalu et al. (2020) [4]	No	1	0	1	English: 1	Yes
Van der Pluijm (1999, 2001) [12, 13]	No	4	0	1	Stretcher: 4	No
Ravenshorst et al. (2016) [14]	No	2	1	1	Stretcher: 2	No
Tapp and Southcombe (1985, 1988) [15]	No	12	8	3	Stretcher: 12	No
Vaculik et al. (2012) [16]	No	4	2	1	Stretcher: 4	No
Vaculik et al. (2017) [17]	No	5	3	1	Stretcher: 5	No
De Vekey et al. (1996) [18]	No	8	5	1	Stretcher: 8	No

2.2. NUMERICAL STRATEGIES TO SIMULATE OUT-OF-PLANE LOADED WALLS

A structure can be modelled in multiple ways. D'Altri et al. devised an extensive collection of modelling strategies for structures. The modelling strategies are divided into categories in figure 2.1. D'Altri summarised the peculiarities of the categories as follows [19]:

1. **Block-based models (BBM)**
   "Masonry is modelled in a block-by-block fashion and, therefore, the actual masonry texture can be accounted for. The block behavior can be considered rigid or deformable, whereas their interaction can be mechanically represented by means of several suitable formulations." [19]

2. **Continuum homogenous models (CHM)**
   "The masonry material is modelled as a continuum deformable body, without distinction between blocks and mortar layers. The constitutive law adopted for the material can be defined either through direct approaches (...) or homogenization procedures and multi-scale approaches." [19]

3. **Geometry-based models (GBM)**
   "The structure is modelled as a rigid body. The geometry of the structure represents the main (or even the only) input of these modeling strategies." [19]

4. **Equivalent frame models (EFM)**
   "The structure is idealized into panel-scale structural components (macroelements) with a phenomenological or mechanical-based response. Typically, two main structural components may be identified: piers and spandrels. The subdivision of the structure into panel-scale portions is an a priori operation made by the analyst who interprets the structural conception of the building." [19]

The categories are not all applicable for the use case of this work. As options 3 and 4 apply to large 3D structures, it is not useful for a single masonry wall. The two remaining categories can both be used to model a masonry wall. The bond pattern is the main parameter which will be studied and therefore a continuum homogeneous model (CHM) is not possible. A CHM simulates the wall as a homogeneous plate, this makes it impossible to model the separate bricks and the mortar joints. Separate bricks and mortar joints can be used to insert the bond patterns into the model. A block-based model is thus the only option to use. Such a block-based model (BBM) will be further discussed in section 2.3. A BBM can also accurately simulate the effect of an out-of-plane load on the wall.

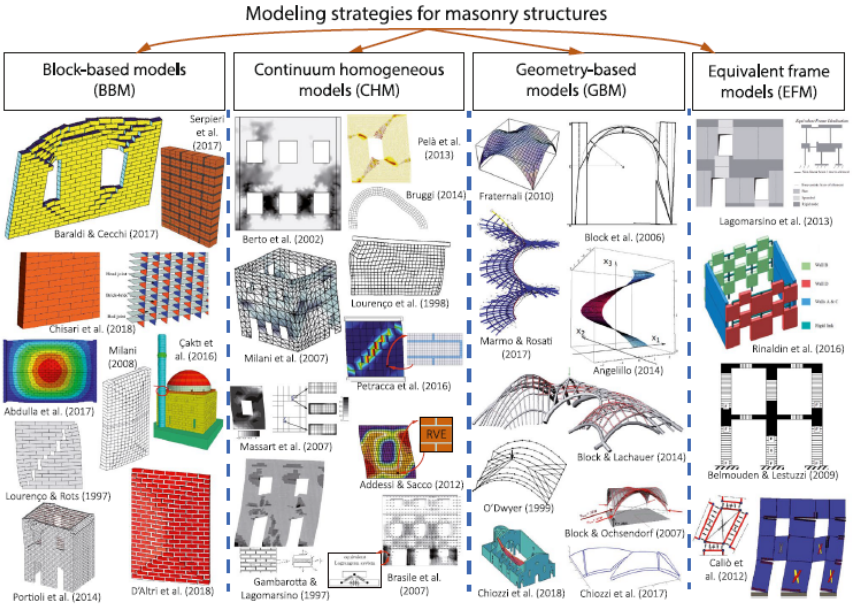

Figure 2.1: Modelling strategies for masonry structures from D'Altri et al. [19]

2.3. BLOCK-BASED MODEL

A block-based model as described in section 2.2 is a model in which the bricks in the masonry wall are modelled separately. The main advantages and disadvantages are listed below [19].

The main advantages are:

- Representation of the actual masonry bond and the structural details
- Mechanical characterization from small-scale experiments
- Clear representation of the failure modes
- The model can account for simultaneous in-plane and out-of-plane responses
- The interaction between orthogonal walls is taken into account

The main disadvantages are:

- The computational demand is very high
- The actual bond of existing masonry structures cannot be completely known
- The assembly of the model is time-consuming

How these bricks and joints are modelled depends on the strategy used. D'Altri et al. subdivides them into five categories [19]. The categories are shown in figure 2.2.

1. **Interface element-based approaches**
   The joints are modelled as zero-thickness elements (with the bricks enlarged to maintain the geometry). The bricks are modelled with a smeared cracking model [19].

2. **Contact-based approaches**
   The contact points between the bricks are governed by a frictional or cohesive-frictional contact definition instead of distinct joints [19].

3. **Textured continuum-based approaches**
   The bricks and joints are modelled separately in a FEM (Finite Element Model) framework without a interface between them. This allows for failure within the brick, within the joint and on the border between the joint and brick [19].

4. **Block-based limit analysis approaches**
   "Block-based limit analysis represents an accurate and robust approach for the prediction of collapse load and failure mechanism of masonry structures." Using static or kinematic theorems of limit analysis. The computational requirements for Block-based limit analysis are very high [19].

5. **Extended finite element approaches**
   The extended finite element method promises to be a valid option that will be able to simulate "the surface-based cohesive behavior to capture the elastic and plastic behavior of masonry joints and [including a model] to simulate the crushing of masonry under compression". The technique is however in its infancy [19].

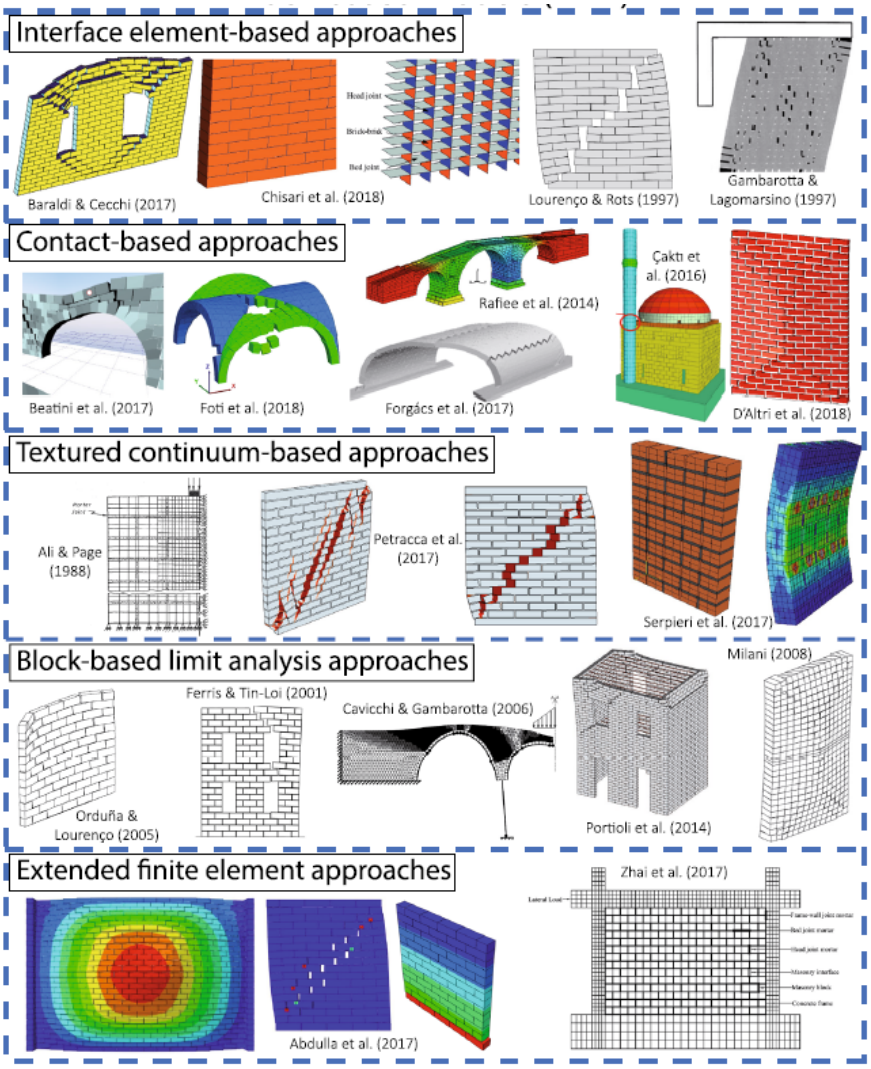

Figure 2.2: Options for a block-based model [19]

3

RESEARCH METHOD

The numerical model is explained in this chapter. Adaptations are made to the numerical model developed by Chang to suit the multiple bond patterns. Firstly, the verification of the model is discussed. The model is calibrated with the data from Griffith et al. [3]. After which the numerical model is explained. The mesh size and type of elements used are discussed, as well as the material properties and the boundary conditions. The assembly of the double wythe masonry wall is also mentioned.
Secondly, the sensitivity study is discussed. This contains an explanation of the cracking model within the bricks and an alternative. The numerical model uses a smeared cracking model, but a discrete cracking model might be a more accurate method. Also, part of the sensitivity study is a mesh sensitivity study. In the numerical model by Chang [1, 2], the face of the brick is divided over its length into two parts, called a halfbrick (Hbrick). This mesh size is too large for the other bond patterns which need at least a division of the face into four parts. Two mesh sizes are compared to the Hbrick and analysed, the quarterbrick (Qbrick) and octogonalbrick (Obrick). After which the effect of the length of the return wall is determined. The end of the return wall is clamped in the experiment and tyings are used in the numerical model to simulate the effect of these clamps. These tyings are removed and the length of the return wall is parameterised.
Lastly, the single and double wythe bond patterns part of this study are shown.

3.1. EXPERIMENTAL BENCHMARK

The numerical and computational model is calibrated and validated by Chang [1] to wall 1 from Griffith et al. [3]. This specimen is part of a study into the effect of openings, the aspect ratio and pre-compression on the out-of-plane bending capacity. The dimensions of the numerical model are matched to the dimensions of the experimental wall and as such the model has similar dimensions and the same pre-compression. The results of the testing campaign were provided to Chang by Griffith who in turn provided the results for this study. The dimensions of the experimental wall are 4 000 x 2 500 mm, the dimensions including the return wall are 4 220 x 2 500 mm. The numerical model in Finite Element

Method (FEM) software Diana is designed and previously used by Chang [1, 2]. The bricks used in the experiment are 230 x 110 x 76 mm. In the numerical model zero-thickness interface elements are used and the bricks are expanded to maintain the global geometry. The zero-thickness interface elements for the mortar joints and the expanded bricks are shown in figure 3.1. The dimensions of the bricks in the numerical model are 240 x 110 x 86 mm, there are 29 courses in the masonry wall. The structural information of the numerical model of the masonry wall is noted in table 3.1.

Table 3.1: Structural information of the numerical model of the masonry wall

Length x Height	4 200 x 2 494 mm
Length of the return wall	480 mm
Size of a brick of main wall	240 x 110 x 86 mm
Size of a brick of return wall	240 x 120 x 86 mm
Pre-compression	0.1 MPa

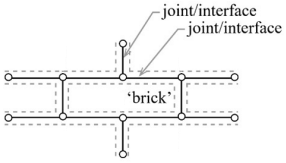

Figure 3.1: A visualisation of the numerical model and the expansion of the bricks [20]

3.2. NUMERICAL MODELLING

The bricks in the return wall are of a slightly different shape, the depth of a brick in the main wall is 110 mm while the depth of a brick in the return wall is 120 mm. As a result, the return wall matches with half a brick of the main wall which makes a cleaner mesh. In the mesh, the bricks are separated in three parts along the width and in four parts over the length. As the brick is halved in the length twice, it is called a quarterbrick (Qbrick). The effect of division into three rows over the depth of the wall instead of other configurations has been studied by Chang [1] and is appropriate. The mesh of a brick is shown in figure 3.2. The mesh of the corner elements is also shown as the mesh is smaller there to connect the mesh of the main wall to the return wall. A clean mesh is maintained for those bricks, except for the centre halfbrick for the double wythe masonry walls (figure 3.2c) as it was not possible to create clean lines.

The bricks are modelled by an isoparametric 3D block element (CHX60) and use Gauss integration. The mortar joints (and the discrete cracks in the bricks) are modelled by a zero-thickness quadrilateral plane element (CQ48I). These elements are shown in figure 3.3. Both use quadratic interpolation.
The double wythe walls are created by assembling additional masonry on the outside of the original single wythe masonry wall. The inner length stays the same at 3 960 mm, the outside length becomes 4 440 mm. The wall is supported in the vertical Z-axis at the bottom by an area support, the bricks are connected by a bed joint to the support. The wall is also prevented from moving in the load-direction by two line supports. These are placed horizontally at the top and bottom of the wall. These two supports are shown in figure 3.4b. Additionally, the wall is supported in the X- and Y-direction by multiple tyings at the end of the return walls. These are discussed further in section 3.3.3.

Before the wall is subjected to an out-of-plane load, the self-weight and pre-compression are applied. The density of masonry is 1900 kg/m^3 and the pre-compression is 0.1 MPa.

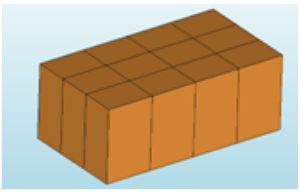

(a) Mesh of a brick

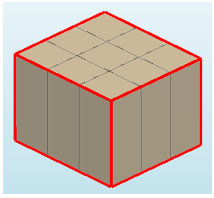

(b) Corner of single wythe wall

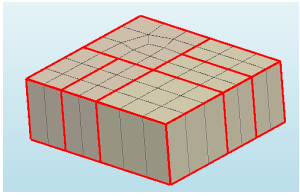

(c) Corner of double wythe wall

Figure 3.2: Details of the mesh of the bricks in the corners

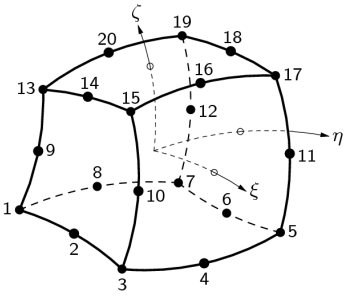

(a) Solid element (CHX60)

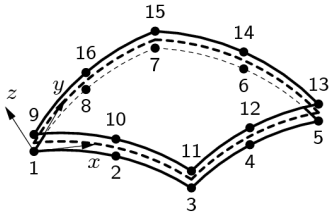

(b) Interface element (CQ48I)

Figure 3.3: Elements used in the numerical model [20]

The pre-compression for the double wythe wall is 0.0478 MPa, this is done to keep the total vertical force equal between the single and the double wythe walls. More extensive material properties of the brick and mortar are summarised in tables 3.2 and 3.3. The cracks within the brick are modelled using a smeared cracking model, this is explained in detail in section 3.3.1. The out-of-plane area load is placed upon the main wall using arc-length control pushing towards the return walls. The arc-length control uses an updated normal plane. Both physical and geometrical nonlinearity are modelled.

The convergence criteria are a force norm at 0.01 and a displacement norm at 0.01. These criteria must both be met to continue to the next load step. If no convergence is reached in 500 iterations will the analysis terminate. The iterative method used is the Quasi-Newton method with the Broyden-Fletcher-Goldfarb-Shanno (BFGS) method. The first tangent used in an iteration is the last one produced in the previous iteration. The solution method used by Diana is the Parallel direct sparse solver. This solver is high-performance and memory-efficient for solving large sparse symmetric and asymmetric linear systems of equations. This solver works well for large numerical models [20].

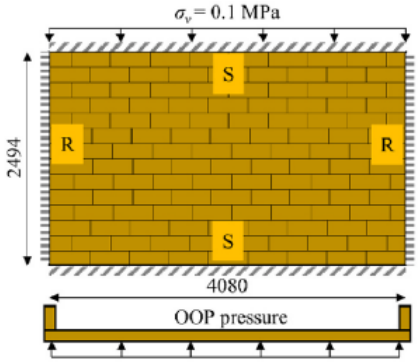

(a) Sketch of the model [2], R means supported by a return wall and S is simply supported

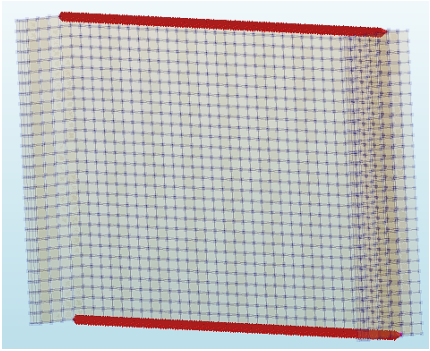

(b) Horizontal line supports along the top and bottom of the wall

Figure 3.4: Sketch of the top view and side view of the numerical model and the horizontal line supports

3.2.1. MATERIAL PROPERTIES

The material properties of the bricks and mortar are shown in tables 3.2 and 3.3. These properties have been calibrated and validated by Chang [1, 2] using the data from Griffith et al. [3]. The total strain crack model is used as the material model for the bricks, this model also implements the smeared crack model. The behaviour of the brick in compression and tension is explained by the compressive and tensile curves entered into the numerical model. These curves are shown in figures 3.5a and 3.5b. The brick is assumed to be elastic in compression, there is no limit to the compressive stress in the brick. This assumption will be validated in section 4.2. The tensile curve is exponential, at first, the tensile resistance increases. However, after softening (cracking) starts to occur within the brick, the strength decreases to zero. A rotating cracking model is used and as such the compressive and tensile curves are valid in all directions. For the interface element, the yield function in figure 3.5c is applied. The yield function includes shear slipping, softening and a compression cap. The interface elements of the bed joints, and head and collar joints are equal, the material properties are the same.

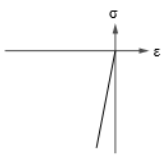

(a) Elastic compressive curve

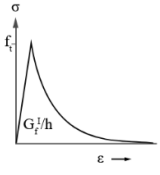

(b) Exponential tensile curve

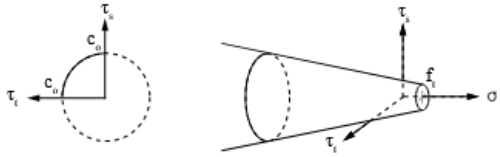

(c) Three dimensional interface yield function

Figure 3.5: Constitutive model of (a,b) the brick and (c) the interface element [20]

Table 3.2: Material properties of the brick [2]

Property	Value
Young's modulus	52 700 N/mm^2
Poisson's ratio	0.16
Mass density	1 900 kg/m^3
Tensile curve	Exponential
Tensile strength	3.55 N/mm^2
Mode-I tensile fracture energy	0.00355 N/mm
Crack bandwidth	10 mm
Residual tensile strength	0
Compression curve	Elastic
Type of crack model	Rotating smeared cracking model

Table 3.3: Material properties of the mortar [2]

Property	Value
Element type	3D structural plane interface
Normal stiffness modulus-z	70 N/mm^3
Shear stiffness modulus-x	30 N/mm^3
Shear stiffness modulus-y	30 N/mm^3
Tensile strength	0.21 N/mm^2
Fracture energy	0.0105 N/mm
Cohesion	0.21 N/mm^2
Friction angle	0.523 rad
Compressive strength	16 N/mm^2
Factor Cs	0.01
Compressive fracture energy	31.5 N/mm
Equivalent plastic relative displacement	0.007

3.2.2. MASONRY GEOMETRY DETAILS

The make-up of the corner details is determined in cooperation with a mason. It was decided to use a staggered pattern. This means that no vertical joint may stretch 2 courses. This results in an alternating pattern and in a connection that is as strong as possible. Additionally, some important assumptions are noted here:

- The height and width of the mortar joints are considered constant
- The thickness of the head joint is considered constant and the head joint is constructed without faults
- The material properties of the head joints are considered equal to the material properties of the bed joints and collar joints, even though this is impossible due to construction methods
- The bricks are identical and without faults

3.3. SENSITIVITY STUDY

In this section, the performed sensitivity studies are explained. Firstly the smeared cracking model within the bricks is discussed, followed by an alternative model, the discrete cracking model. Secondly, the options for the mesh of the brick and motivation for the mesh size and its sensitivity study are discussed. Lastly, the boundary conditions of the experiment by Griffith et al. [3] are discussed and their implementation into the numerical model.

3.3.1. CRACKING MODEL WITHIN THE BRICK

Chang's model makes use of a smeared cracking model. In Diana, the cracking model is explained as "The smeared crack models consider cracking as a distributed effect with directionality and cracked material is simulated as a continuous medium with anisotropic characteristics" [20]. The crack in the brick is spread out over the element and its exact location is unknown. This is contrary to a discrete cracking model where the location of the crack is determined by the user. The discrete crack forms a discontinuity within the brick. Including this in the model might yield more accurate results, as the experiments by Griffith et al. [3] and Padalu et al. [4] showed cracks propagating vertically through the bricks. In the case of a masonry wall, the location of the cracks can be determined quite accurately. The cracks will likely occur in the joints (vertical and horizontal) and vertically straight through the brick. The possible locations of the cracks are shown in figure 3.6a of a stretcher bond. The joints are already an interface element and as such a crack can propagate through the brick.

The discrete cracking model is implemented into the model by separating the bricks into two pieces and placing discrete interface elements in between the two pieces. Due to the removal of smeared cracking, the brick will behave completely elastic (in compression and tension). The data of the discrete crack interface element is noted in table 3.4. The stiffness of the interface is determined using a dummy stiffness: $k = 1000E/l$. Where E is the Young's modulus of the brick and l is the length of the element. The tensile curve according to Hordijk et al. (figure 3.6b) is used for tension softening as the exponential curve is unavailable and it is very similar to the exponential curve (figure3.5b) originally used for the bricks.

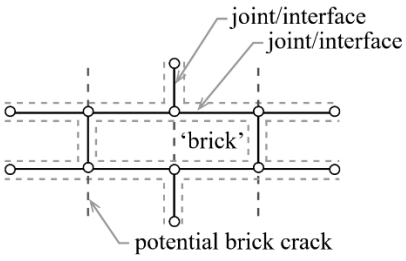

(a) Visualisation of discrete crack locations [20]

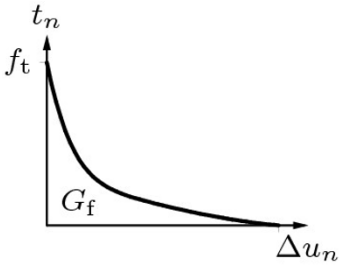

(b) Hordijk et al. tensile curve [20]

Figure 3.6: The location of the discrete crack and the Hordijk et al. tensile curve

Table 3.4: Material information of the discrete crack interface within the brick

Property	Value
Element type	3D surface interface
Dummy normal stiffness modulus-z	439 167 N/mm^3
Dummy shear stiffness modulus-x	189 300 N/mm^3
Dummy shear stiffness modulus-y	189 300 N/mm^3
Tensile strength	3.55 N/mm^2
Fracture energy	0.00355 N/mm
Mode-I tension softening criterion	Hordijk et al.[20]
Mode-I unloading/reloading model	Linear elastic
Mode-II shear criterion for crack development	Zero shear traction

3.3.2. MESH SENSITIVITY STUDY

A mesh sensitivity study is performed to determine the effect of the mesh size of the bricks. The mesh size used by Chang [1, 2] cannot be used as the bonding patterns have an overlap per brick of 1/4, 1/2 and 3/4. Chang's model uses halfbricks (Hbrick) as shown in figure 3.7a which can only do an overlap of 1/2. This requires a change in the model to a smaller mesh size. The quarterbrick mesh (Qbrick) is preferable as it requires the smallest change and increases the number of nodes and elements the least, shown in figure 3.7b. An octagonalbrick mesh (Obrick) is also studied (shown in figure 3.7c) which maintains the aspect ratio of the Hbrick. The significance of these three mesh sizes will be determined in chapter 4.

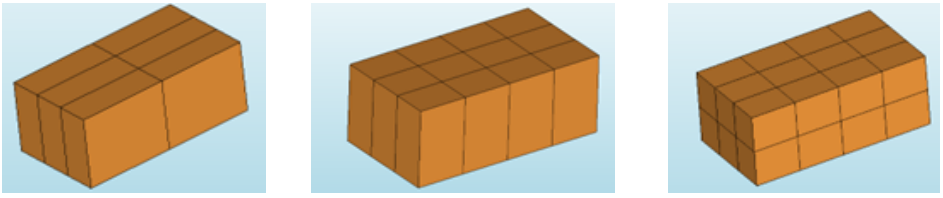

(a) Halfbrick (Hbrick) (b) Quarterbrick (Qbrick) (c) Octagonalbrick (Obrick)

Figure 3.7: Mesh of a single brick

3.3.3. BOUNDARY CONDITIONS OF THE RETURN WALLS

The length of return walls also influences the capacity of the masonry wall. Chang et al. [1, 2] used a return wall length of 480 mm just as the testing campaign from Griffith et al. [3]. In the experiment, the end of the return walls were clamped using C-shaped channels to prevent any translation and rotation. The clamping of a return wall is shown in figure 3.8a. To simulate the clamps, tyings are added into the model. These tyings are lines spanning from the bottom course to the top course along the end of the return walls, and for all points on the line can any or more translations and rotations be equalised. There are five such tyings present in the model and these are shown in figure 3.8b. Four of these tyings equalise the translation in both horizontal directions. There is one special tying that only

stops the horizontal movement perpendicular to the load direction, this is to prevent any global movement of the entire masonry wall [2]. The four normal tyings are situated at the corners of the end of the return walls, the location of these tyings also restrains the rotation. The fifth tying is situated in the middle of the end of the return wall (right return wall in figure 3.8b). As these tyings are connected to the mortar joint between the bottom course and the vertical support all movement is prevented. The effect of these tyings and the length of the return wall can be determined by removing the tyings and to parameterise the length of the return wall. The assembly of the double wythe walls included adding additional tyings to maintain this clamping.

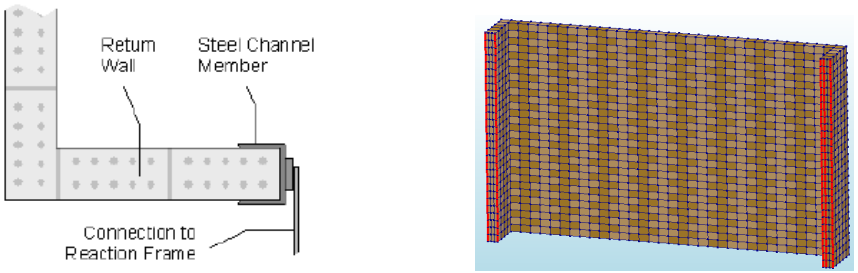

(a) Top view of the return wall in the experiment [3]

(b) Location of tyings in the model

Figure 3.8: Details on the end of the return wall

3.4. OVERVIEW PARAMETRIC STUDY

The bond patterns which will be examined in this study are shown in figure 3.9. These consist of five single wythe patterns (figure 3.9a - 3.9e) and three double wythe patterns (figure 3.9f - 3.9h). All the patterns are symmetric except for the lateral bond (figure 3.9b).

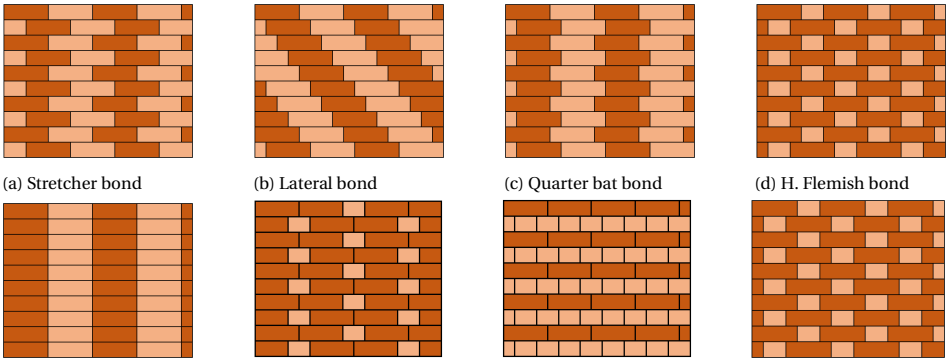

(a) Stretcher bond

(b) Lateral bond

(c) Quarter bat bond

(d) H. Flemish bond

(e) Stack bond

(f) Chain bond

(g) English bond

(h) Flemish bond

Figure 3.9: The bond patterns visualised, bond patterns (a) - (e) are single wythe and bond patterns (f) - (h) are double wythe

4

NUMERICAL RESULTS

In this section, the reference model is introduced and compared to an experimental benchmark by Griffith et al. [3]. Firstly, the compressive behaviour of the bricks is analysed. As the validity of the numerical model depends on the absence of crushing within the brick. A mesh sensitivity study will also be performed, as the mesh size of the bricks has changed compared to the model of Chang. The type of cracking model will also be examined as currently there is no cracking through the brick, however experimental results have shown that cracks can propagate through the brick. Finally, will the lateral boundary conditions be studied. The length of the return wall as well as the boundary condition at the end of the return wall do influence the out-of-plane bending capacity.

4.1. REFERENCE MODEL

The reference model that is used in this study is adapted from Chang [2]. The dimensions of the experiment are shown in figure 4.1. The load-displacement curve of the experiment is shown in figure 4.2 and matches well with the numerical model. The model and the experiment are identical until the out-of-plane two-way bending capacity is reached. The two-way bending capacity in the experiment is 4 757.8 Pa compared to 4 764.0 Pa for the numerical model, the stiffness of the masonry is also the same. There is however a different post-peak. The experiment plateaus on a higher load level. The numerical model stops at 18 mm, the analysis is unable to reach convergence after with its set limit of 500 iterations. The experiment can reduce the load to zero without failure. The crack pattern obtained by Griffith et al. [3] is shown in figure 4.3b and is also identical to the crack pattern of the numerical model shown in figure 4.3a. The same cross-yielding pattern is present. There is however a vertical crack through the brick in the return wall. This crack is not present in the computational model, an attempt to recreate this is shown in section 4.3.2. The crack pattern from the experiment is taken after the test while the crack pattern for the model is taken at the last load step that reached convergence. The number of iterations per load step is shown in Appendix A for all bond patterns and the additional studies part of this section.

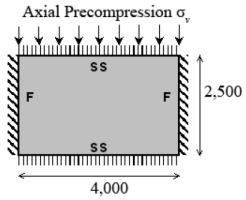

(a) Side view

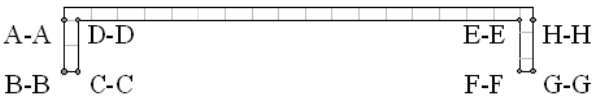

(b) Top view

Figure 4.1: Dimensions of masonry wall of Griffith et al. [3], with SS = simply supported and F = fixed support (return wall)

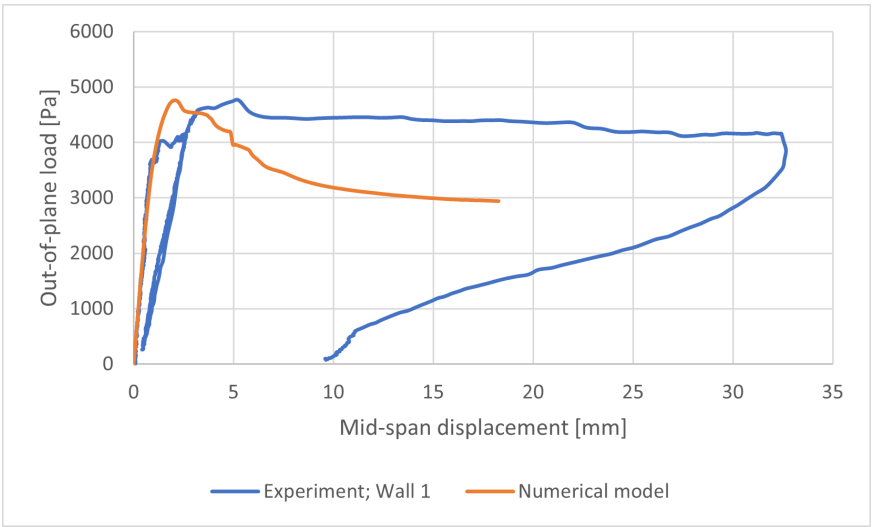

Figure 4.2: Load-displacement of Griffith et al.'s experiment and the numerical model

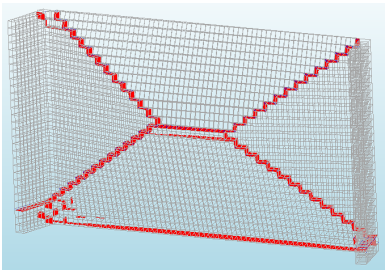

(a) Crack pattern of the reference model

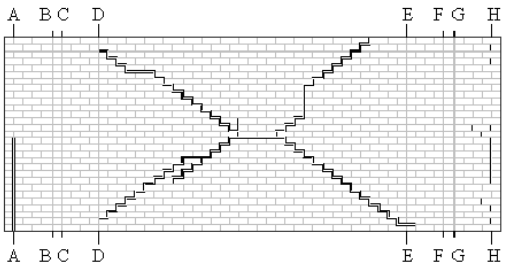

(b) Crack pattern at the conclusion of the experiment by Griffith et al [3], top view is shown in figure 4.1b

Figure 4.3: Crack patterns from the numerical model at the last point before nonconvergence, deformation scale factor = 20, the crack pattern is created using DUNz removing all relative displacements below 0.2 mm and the experimental results of wall 1 from Griffith et al. [3]

4.2. COMPRESSIVE BEHAVIOUR OF THE BRICK

The material properties of the bricks in the model assume that the brick behaves elastically under compression (table 3.2). This is accurate as long as the compressive stresses do not exceed the characteristic compressive strength of the bricks. When compressive strength is exceeded, nonlinear effects like crushing will appear, which the numerical model does not take into account. As a result, the numerical model would no longer be accurate. The compressive strength of the masonry used by Chang et al. [1, 2] and Griffith et al. [3] is 16 MPa. The compressive stresses in the model must be lower than this to not run into the model's limitation.

In figure 4.4 are two contour plots of the minimum principal stresses shown, all tensile stresses and compressive stresses lower than 1.50 MPa are removed. The compressive stresses are generally very low. There are in both models two points where the compressive stress spikes, these are highlighted in each contour plot. The minimum principal stress recorded is 11.35 MPa and 15.18 MPa for the single wythe and double wythe masonry wall, respectively. These stresses occur post-peak. Even if the compressive stress would exceed the compressive strength of the brick, the out-of-plane two-way bending capacity would not be influenced. For the stretcher bond, the compressive stress spikes at the left return wall in the top and bottom courses. The Flemish bond spikes at both corners in the top course. The spots are half a brick from the inside corner and are at a location of a mortar joint. The bricks rotate around these points to increase resistance. The reason for a spike at the bottom course for the stretcher bond is the absence of a mortar joint half a brick from the return wall in the top course on the other side. For both cases was after this load step a severe decrease in compressive stress noticed, this is due to a mortar joint giving way somewhere else within the masonry structure. The check for compressive behaviour is satisfied as both compressive stresses were less than the maximum of 16 MPa.

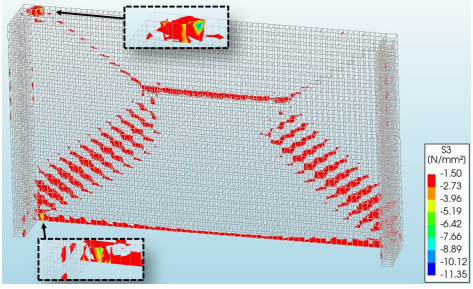

(a) Stress contour plot on the load step (4 503 Pa, post-peak) with stretcher bond

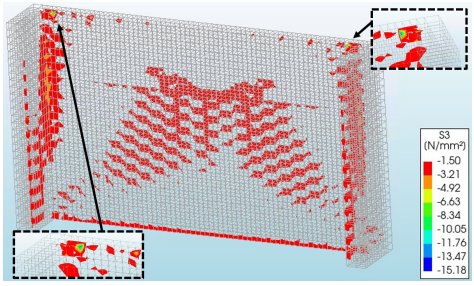

(b) Stress contour plot on the load step (15 513 Pa, post-peak) with Flemish bond

Figure 4.4: Compressive stresses in the model for 2 bond patterns, all tensile stresses and compressive stresses lower than 1.50 MPa are removed

4.3. SENSITIVITY STUDY

In this section, the sensitivity study is performed and are the results discussed. First is the mesh sensitivity study analysed, as a change in mesh size of the brick is required to implement the bond patterns. Secondly, the sensitivity of the crack model within the bricks is determined. Two options are analysed, the smeared cracking model and the discrete cracking model. At last is the effect of the boundary conditions investigated. In the experiment by Griffith et al. [3], the end of the return walls are clamped while in the numerical model this is abstracted by the use of tyings.

4.3.1. MESH SENSITIVITY STUDY

The crack patterns are shown in figure 4.5 for a mid-span displacement at 3 mm and at the maximum reached mid-span displacement, the load displacement curve is shown in figure 4.6. For the Obrick, the 3 mm mid-span displacement was the last step before nonconvergence. At a mid-span displacement of 3 mm the crack patterns of the Hbrick and Qbrick are almost identical while the Obrick has a more filled out pattern. The mesh of the Obrick contains more nodes and elements and has become complex. The length of the analysis of the Obrick is significantly shorter as the maximum mid-span displacement is 3 mm while the Hbrick and Qbrick continued the analysis until a mid-span displacement of 18.5 mm and 15.5 mm, respectively. The crack patterns of the Hbrick and Obrick at their maximum mid-span displacement is shown in figure 4.5b and 4.5d. The crack patterns at the last step before nonconvergence are almost identical. As shown in the load-displacement curve, the responses are the same between the different mesh sizes. The out-of-plane bending capacity, mid-span displacement and initial stiffness are similar. There is no discernible difference between the mesh sizes. However, the Obrick is more difficult to reach convergence and increased computational time significantly. The data of the load-displacement curve is summarised in table 4.1. The Qbrick can thus be used for the analysis of the bond patterns.

Table 4.1: Results for the multiple mesh sizes at force capacity

Mesh size	Bending capacity		Mid-span displacement		Initial stiffness
Hbrick	4 727.7 Pa	100%	2.035 mm	100%	4 367.5 N/mm^3
Qbrick	4 764.0 Pa	100.7%	2.040 mm	100.3%	4 356.6 N/mm^3
Obrick	4 779.8 Pa	101.1%	2.054 mm	100.9%	4 325.3 N/mm^3

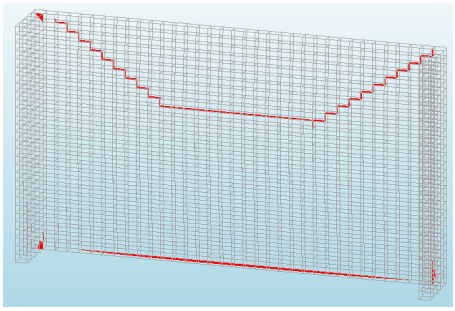

(a) Hbrick at mid-span displacement of 3 mm

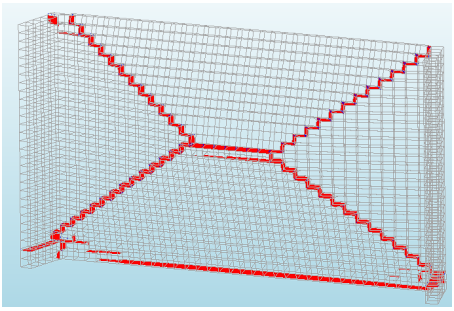

(b) Hbrick at the last step before nonconvergence

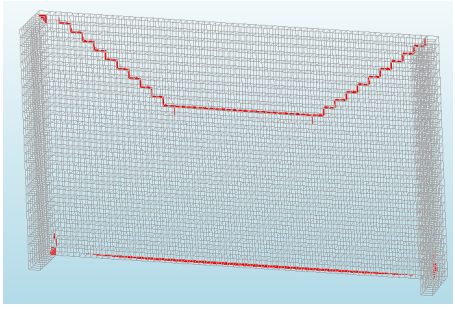

(c) Qbrick at at mid-span displacement of 3 mm

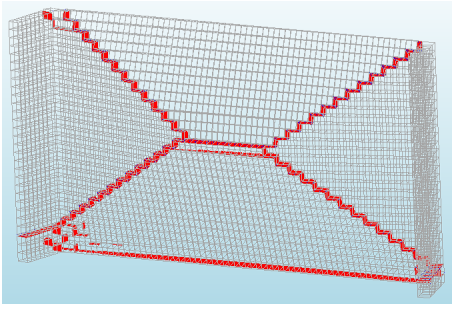

(d) Qbrick at the last step before nonconvergence

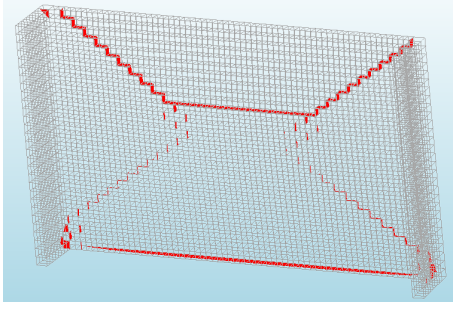

(e) Obrick at mid-span displacement of 3 mm

Figure 4.5: Crack patterns of the mesh sensitivity study, deformation scale factor = 20, the crack pattern is created using DUNz removing all relative displacements below 0.05 mm for mid-span displacement of 3 mm and below 0.2 mm at the last step before nonconvergence

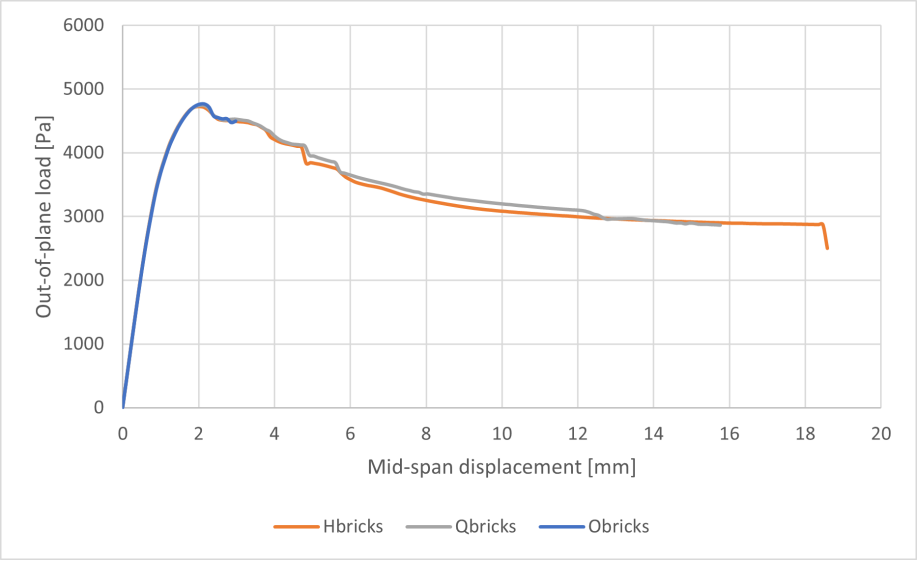

Figure 4.6: Load displacement curve for the Hbrick, Qbrick and Obrick

4.3.2. SENSITIVITY OF THE CRACK MODEL FOR TENSILE FAILURE WITHIN THE BRICK

A crack in a masonry wall can be modelled in two ways. Chang et al. [2] uses a smeared cracking model, an alternative is a discrete cracking model. The discrete cracking model might be able to simulate to vertical cracks through the bricks as observed in the experiments by Griffith et al. [3] and Padalu et al. [4]. In a discrete cracking model are the crack locations predetermined by the user.

The effect of the cracking model on the load-displacement curve is shown in figure 4.7 with the results in table 4.2. The two-way out-of-plane bending capacity of the wall is very similar for the smeared and discrete cracking model. There is a however an 8% difference in mid-span displacement, this difference does not change the initial stiffness but moves the bending capacity to a point of greater mid-span displacement. This is shown in figure 4.8a. The behaviour of the wall does change, the wall behaves more like a plate. The cracks, however, do still follow the mortar joints at the same slope as the smeared cracking model (figure 4.8a). The discrete cracks do not open a new avenue for the cracks to propagate. This can be explained by relatively strong bricks compared to the mortar.

An additional negative is the difficulty to reach convergence when a discrete cracking model is used. The convergence graph is shown in figure A.1a in Appendix A. Beyond 77 load steps no convergence is reached after 500 iterations. This is not the point of failure of the wall but does show the instability of the model. An attempt to continue with the next load steps despite the previous nonconvergence, has been performed, these additional load steps also did not reach convergence in 500 iterations either.

Table 4.2: Results for smeared and discrete cracking model, mid-span displacement taken at out-of-plane bending capacity

Cracking model	Bending capacity		Displacement		Initial stiffness
Smeared cracking	4 727.7 Pa	100%	2.035 mm	100%	4 367.5 N/mm^3
Discrete cracking	4 755.6 Pa	100.6%	2.212 mm	108.7%	4 366.8 N/mm^3

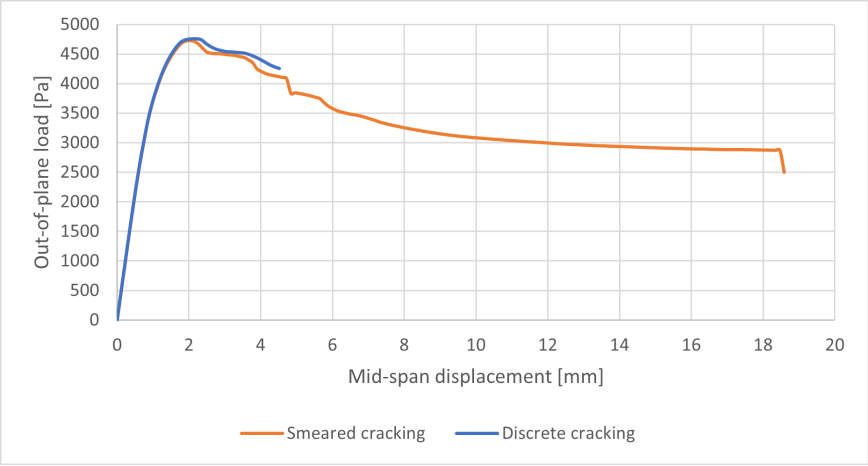

Figure 4.7: The load-displacement curve of smeared and discrete cracking within the brick

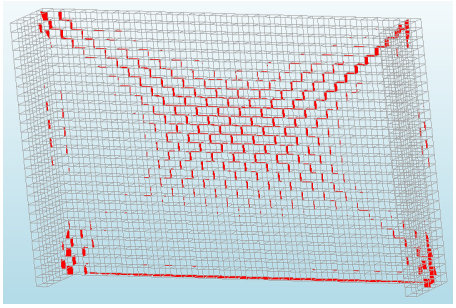

(a) Discrete cracking model

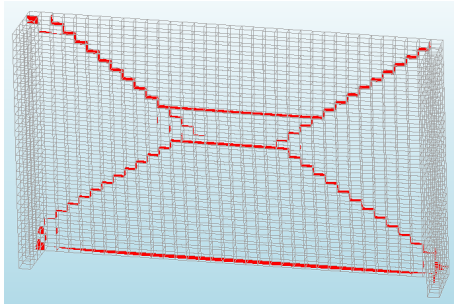

(b) Smeared cracking model

Figure 4.8: Crack patterns of the sensitivity of the crack model within the brick at a mid-span displacement of 4.5 mm, deformation scale factor = 20, the crack pattern is created using DUNz removing all relative displacements below 0.05 mm

4.3.3. LATERAL BOUNDARY CONDITIONS

Many different set-ups are used in the experiments from table 2.1. The type and length of the return wall can also be parameterised. Chang et al. [2] uses a mixture of a return wall with tyings at the end to simulate the clamped edges as used by Griffith et al. [3]. In this separate analysis the tyings are removed as these tyings are present to equalise the movement along a line over the height of the end of the return wall. The tyings are shown in figure 3.8b. A range from 1 Hbrick to 10 Hbricks has been analysed. The results are shown in table 4.3. Figure 4.9 shows the out-of-plane bending capacity for each length of the return wall and the clamped edge as a dashed line. The shortest return walls are significantly less effective but after at least 5 Hbricks does the capacity approach the clamped situation. The crack pattern shown in figure 4.10 corroborates this statement. The 1 to 5 Hbricks show a progression from fully one-way bending to two-way bending. The 1 Hbrick return wall (= 0 mm, figure 4.10a) has only two cracks in the structure, a crack horizontally at the bottom in the joint on the support and a crack horizontally in the middle of the wall. Due to the lack of supports on the vertical edges are both vertical edges free. The horizontal crack in the middle of the wall is present on lengths from 1 Hbrick to 4 Hbricks. As the length of the return wall is increased does the cross-yielding pattern appear and decreases the size of the the horizontal crack in the middle of the wall. Using 5 to 8 Hbricks (figure 4.10e) and using 9 and 10 Hbricks (figure 4.10f) have similar crack patterns. All lengths longer than 5 Hbricks have a box in the centre of the crack pattern and a horizontal crack through the box is present for lengths of 9 and 10 Hbricks. This does not influence the out-of-plane bending capacity. The unclamped situation will however never reach the clamped situation. The clamping is a good enough approximation for situations which can be found in actual structures as the length is often much longer than 5 Hbricks (= 480 mm). The load-displacement curve is shown in figure B.1 in Appendix B.

Table 4.3: Out-of-plane bending capacity for multiple return wall lengths

Length of return wall		Bending capacity
1 Halfbrick (no return wall)	0 mm	2 300.0 Pa
2 Halfbricks	120 mm	2 858.4 Pa
3 Halfbricks	240 mm	3 481.3 Pa
4 Halfbricks	360 mm	4 066.3 Pa
5 Halfbricks	480 mm	4 284.1 Pa
6 Halfbricks	600 mm	4 307.5 Pa
7 Halfbricks	720 mm	4 332.4 Pa
8 Halfbricks	840 mm	4 350.7 Pa
9 Halfbricks	960 mm	4 364.3 Pa
10 Halfbricks	1 080 mm	4 376.7 Pa
Clamped and immovable with 5 Half bricks	480 mm	4 727.7 Pa

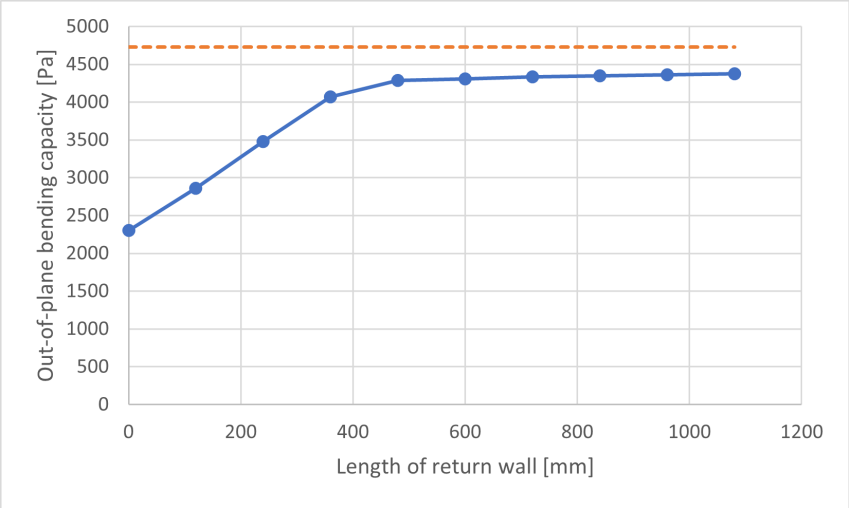

Figure 4.9: Visualisation of bending capacity approaching clamped situation as the length of the return wall increases

4.4. CONCLUDING REMARKS

The assumption by Chang about the compressive behaviour of the bricks has been analysed and a sensitivity study has been performed. Firstly, will the assumption be discussed and afterwards are the results of the sensitivity study evaluated. The model adapted from Chang can be used as crushing is not an issue, the compressive stress remains below the compressive resistance of the bricks. The spikes of compressive stress occur half a brick from the return wall at the point of greatest rotation due to global deformation of the structure. As the brick in the corner is unable to rotate because it is connected to the return wall. The wythe of the wall does influence the compressive stress; however, it is not a problem in this study. The addition of a wythe increases the compressive stress within the bricks. It will become a problem for masonry walls with a wythe greater than two.

The change of mesh size to quarterbricks (Qbricks) is possible and does not lead to any differences in out-of-plane bending capacity and initial stiffness. Each decrease in mesh size does increase computational time and makes reaching convergence more difficult, the mesh is becoming too complex. This is not a problem for the Qbricks yet, but the use of octogonalbricks (Obricks) makes obtaining any conclusive data hard. The crack patterns are almost identical. The length of the analysis due to convergence difficulty impacts the visibility of the crack patterns. The crack pattern has not filled-out completely. The out-of-plane two-way bending capacity of all three mesh sizes is similar. The shape of the load-displacement curve is identical.

On the contrary, the discrete cracking model for the bricks is not used as the cracks still go through the joints, the bricks stay intact. Additionally, the numerical model with a discrete cracking model does not reach convergence quickly (or at all). The out-of-plane bending capacity of the masonry wall does not change compared to the smeared cracking model. The lack of cracks in the brick can also be explained by the use of strong clay

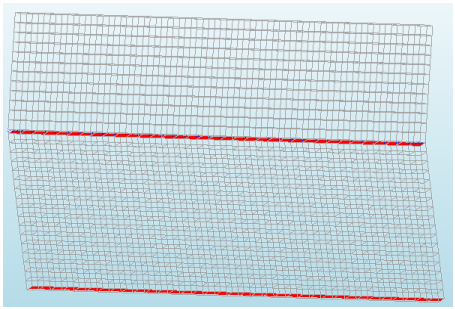

(a) 1 Halfbrick

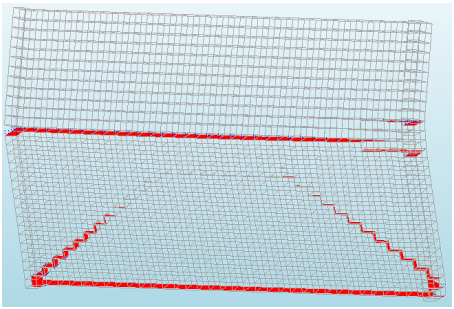

(b) 2 Halfbricks

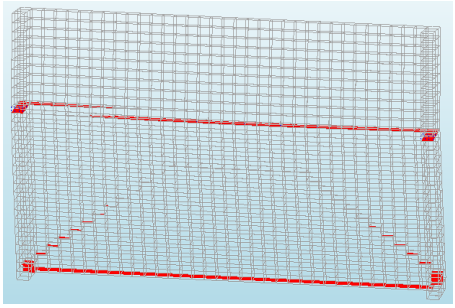

(c) 3 Halfbricks

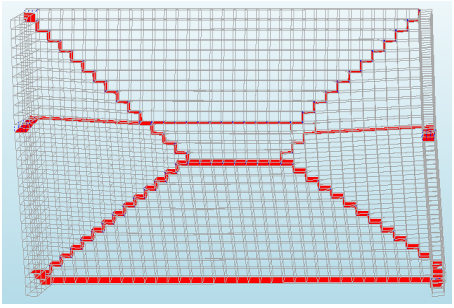

(d) 4 Halfbricks

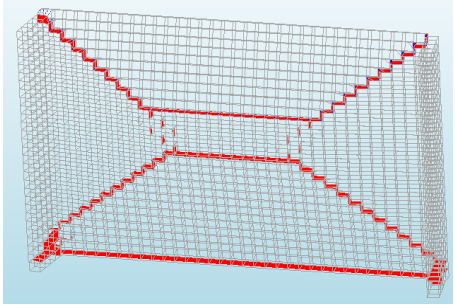

(e) 5 Halfbricks

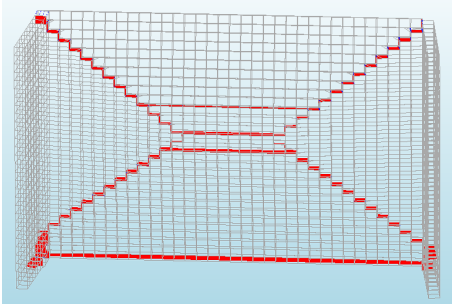

(f) 9 Halfbricks

Figure 4.10: Crack pattern at point of nonconvergence of multiple different length of the return wall, the force upon the wall is the last step before nonconvergence, deformation scale factor = 20, the crack pattern is created using DUNz removing all relative displacements below 0.2 mm

bricks together with relatively weak mortar. A different mix of materials might result in different behaviour.
Lastly, the boundary condition of the return wall is accurate and acceptable. The response of a masonry wall without a return wall changes into one-way bending. Return walls of lengths of 0 to 480 mm show a transition from one-way bending to two-way bending while lengths longer than 480 mm are solely two-way bending. The out-of-plane bending capacity increases in the transition from one-way to two-way bending. As two-way bending is reached, the out-of-plane bending capacity stops increasing and is equal to all longer lengths. The return wall of 10 Hbricks with no additional tyings has an out-of-plane bending capacity which is only 7.5% lower than the clamped situation. The clamped situation is thus a close approximation. Return walls in built structures are often much longer.

5

PARAMETRIC STUDY

This chapter determines the out-of-plane bending capacity of all bond patterns part of this study. These out-of-plane bending capacities are analysed using load-displacement curves. Additionally, the crack patterns are produced. Subsequently, all bond patterns are compared using these two data sources. From these sources, the initial stiffness and the slope of the crack pattern are determined which will be used to explain the effect of the bond pattern on the out-of-plane bending capacity of masonry walls.

5.1. SINGLE WYTHE BOND PATTERNS

The two-way out-of-plane capacity of the single wythe bond patterns are shown in figure 5.1 and are noted in table 5.1. While the out-of-plane bending capacity is similar across all bond patterns, the bending capacity peaks at different mid-span displacements. The stiffness of the bond patterns diverges after an out-of-plane load of 2 500 Pa. This results in a bending capacity at a higher mid-span displacement for the half Flemish bond and the stack bond. The lateral bond surprisingly has the lowest out-of-plane bending capacity (and not the stack bond), and the half Flemish bond is the highest of the single wythe bond patterns. Post-peak is the behaviour different between all the bond patterns. The cracks propagate at other load levels as the location of the mortar joints differs between bond patterns. The post-peak line does not flow smoothly as new cracks result in sudden decreases in out-of-plane loads.

Table 5.1: The out-of-plane bending capacity of the single wythe bond patterns

Bond pattern	Capacity
Stretcher bond	4 762.3 Pa
Lateral bond	4 651.1 Pa
Quarter bat bond	4 744.7 Pa
Half Flemish bond	4 916.0 Pa
Stack bond	4 689.9 Pa

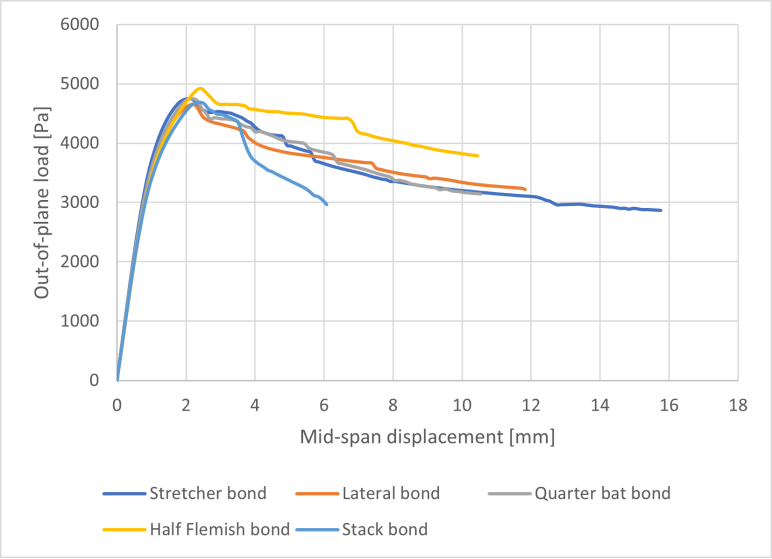

Figure 5.1: The load-displacement curve of all single wythe bond patterns

The crack patterns which are part of this section are shown in figure 5.3a-5.3e. The shape of the crack patterns is similar except for the stack bond. The stack bond has no discernible pattern. The other four bond patterns crack horizontally in the mortar joint between the vertical support and the lowest course and produce a cross-yielding pattern. The quarter bat bond and the half Flemish bond have a box in the centre of the cross-yielding pattern, while this is absent with the lateral bond. The stretcher bond is an intermediary, there is another horizontal crack one row below the central crack. The lateral bond has the only crack pattern (of the four with a cross-yielding pattern) which is not smooth and symmetric, this is due to the bond pattern which is asymmetric as well. The diagonal cracks do exactly stop at the top corners but at the bottom corners, the crack goes around the corner and continues horizontally in the return wall. The bond patterns are shown again in figure 5.2.

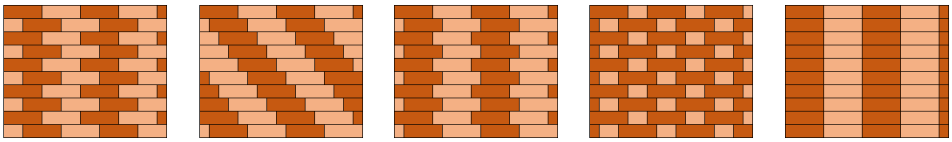

(a) Stretcher bond (b) Lateral bond (c) Quarter bat bond (d) H. Flemish bond (e) Stack bond

Figure 5.2: Single wythe bond patterns visualised

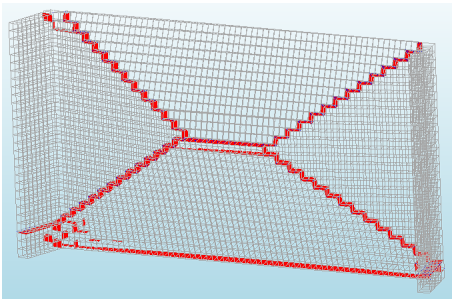

(a) Stretcher bond

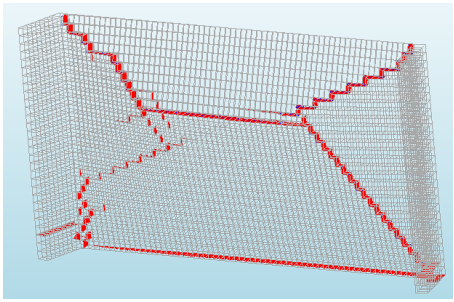

(b) Lateral bond

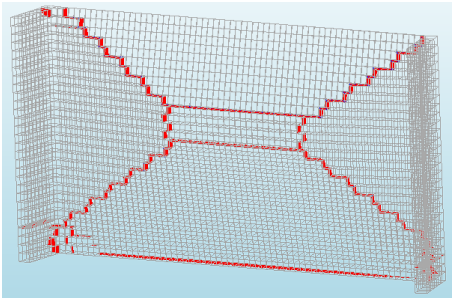

(c) Quarter bat bond

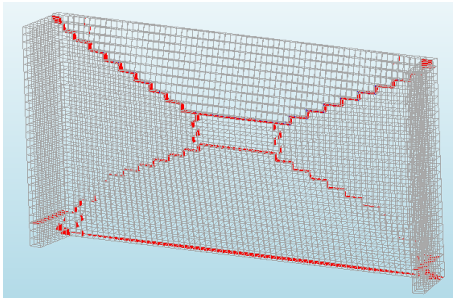

(d) Half Flemish bond

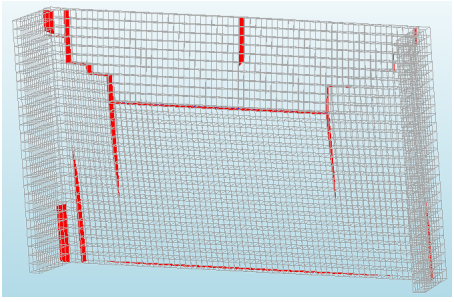

(e) Stack bond

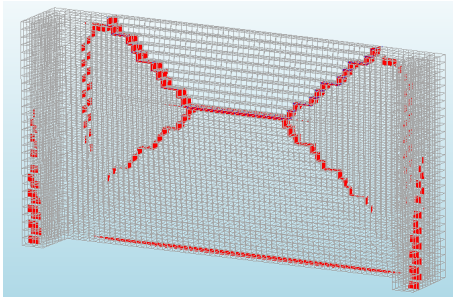

(f) Chain bond

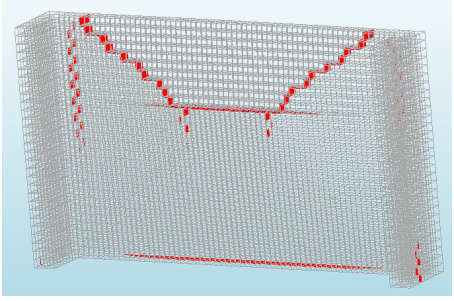

(g) English bond

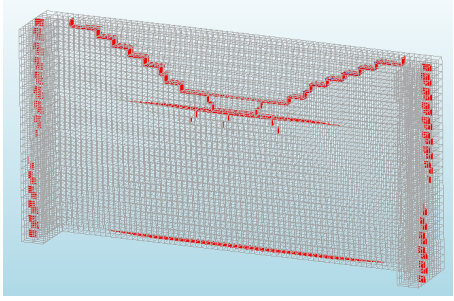

(h) Flemish bond

Figure 5.3: Crack pattern of all bond patterns, the force upon the wall is the last step before nonconvergence, deformation scale factor = 20, the crack pattern is created using DUNz removing all relative displacements below 0.2 mm

5.2. DOUBLE WYTHE BOND PATTERNS

The same analysis of section 5.1 is done for the double wythe bond patterns, the bond patterns are shown again in figure 5.4. The out-of-plane two-way bending capacities of the bond patterns are shown in table 5.2 and the load-displacement curve is shown in figure 5.5. The chain bond and Flemish bond have a very similar shape at the beginning of the load-displacement curves, but the chain bond peaks at an out-of-plane bending capacity of 17 800 Pa. The Flemish bond continues to its out-of-plane bending capacity of 18 741 Pa. The crack patterns are also shown in figures 5.3f-5.3h. Contrary to the single wythe bond patterns, the double wythe bond patterns do produce vertical cracks, these cracks in the return walls still go through the mortar joints though.

For a qualitative comparison, the experiment by Padalu et al. [4] is considered. Only the crack pattern (both faces of the main wall are shown in figure 5.6b) can be considered as the shape and size of their experimental wall and the type of loading is significantly different. In the experimental campaign by Padalu et al. [4] multiple walls were tested, however, only one is unreinforced and without other additional composite materials. The bond pattern used is the English bond. Contrary to the numerical test performed in this study, Padalu et al. uses reversed cyclic loading, which means that the load-direction constantly flips. The wall therefore has another geometry as shown in figure 5.6a. The experimental wall is only restrained at the top and bottom, not over the height of the end of the return wall. The compressive strength of the masonry is also significantly weaker at 7.5 MPa while the masonry structure from Chang [1, 2] has a compressive strength of 16 MPa [3]. The severely weaker structure changes the behaviour and the crack pattern. In comparison to the numerical study has the crack pattern a similar slope of the cross-yielding pattern. The cross-yielding pattern has not developed completely, a triangle shape has appeared in one bottom corner. The slope of the crack pattern is similar to the slope observed in the analysis, the slope of the crack pattern will be further discussed in section 5.3. It does however not have a clean cross-yielding pattern nor is the pattern symmetrical. The cracks in the return wall are horizontal just as in some single wythe bond patterns. Vertical cracks through the bricks are also present in this experiment. The top horizontal crack is absent in the model, this is due to the restraints used by Padalu et al.

Table 5.2: The out-of-plane bending capacity of the double wythe bond patterns

Bonding pattern	Capacity
Chain bond	17 757 Pa
English bond	17 392 Pa
Flemish bond	18 741 Pa

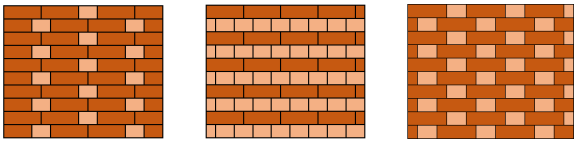

(a) Chain bond (b) English bond (c) Flemish bond

Figure 5.4: Double wythe bonding patterns

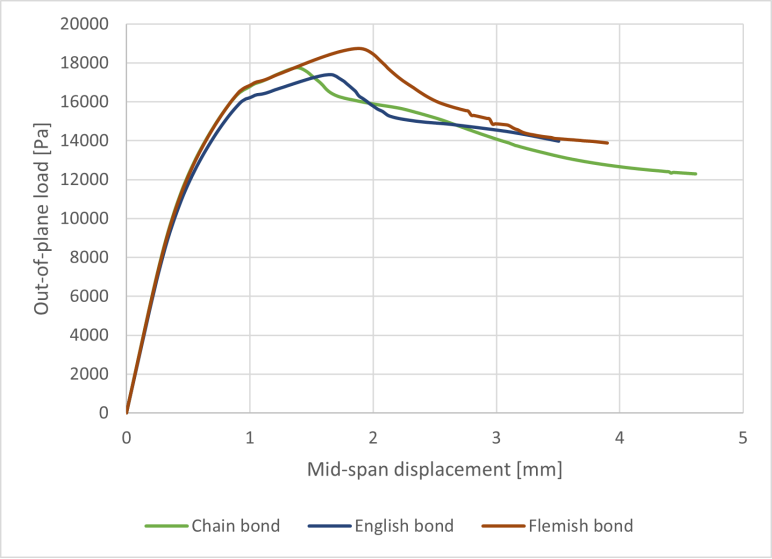

Figure 5.5: The load-displacement curve of all double wythe bond patterns

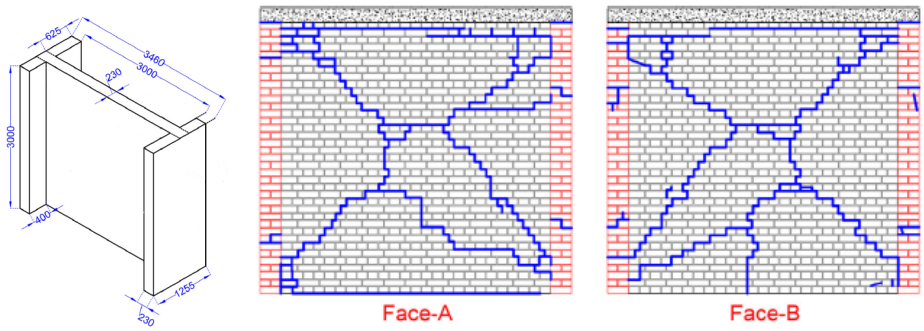

(a) Drawing of the wall used by Padalu et al. [4]

(b) Crack pattern of the main masonry wall of the test performed by Padalu et al., the excerpt is from figure 18b [4]

Figure 5.6: Dimensions and crack pattern of the experiment performed by Padalu et al.

5.3. COMPARISON BETWEEN ALL BOND PATTERNS

The out-of-plane bending capacities for all bond patterns part of this study have been determined in the previous sections. Additionally, other than the difference in wythe is the vertical pre-compression also different. The vertical pre-compression for the single wythe and double wythe is 0.1 MPa and 0.0478 MPa, respectively. This is to maintain an equal vertical force between the two situations. The pre-compression does influence the out-of-plane bending capacity as shown in the experiments by Griffith et al. A higher pre-compression results in a higher out-of-plane bending capacity [3]. All the load-displacement curves of the bond patterns are shown in figure 5.7. The difference in

out-of-plane bending capacities of the single compared to the double wythe stands out immediately. The highest out-of-plane bending capacity of the single wythe bond patterns is the half Flemish bond with 4.92 kPa and the highest out-of-plane bending capacity of the double wythe bond pattern is the Flemish bond with 18.7 kPa. The spread of the out-of-plane bending capacities is 0.27 kPa or 5.4% and 1.3 kPa or 7.2% respectively. The spread within the number of wythe is small. The wythe is more significant, as the doubling and interlocking resulted in a strength increase of 280%.

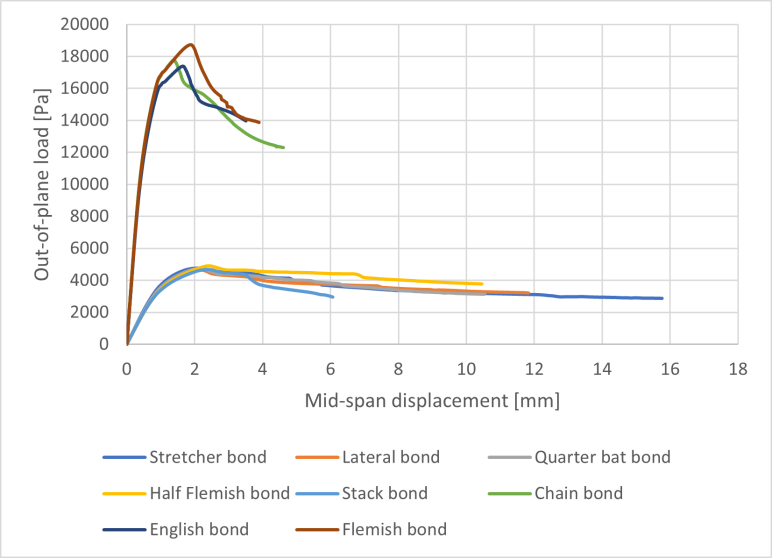

Figure 5.7: The load-displacement curve of all bond patterns

The results of the single and double wythe can be compared not just by the out-of-plane bending capacity. Other statistics which can be compared are the initial stiffness and the slope of the crack pattern. These two values give more insight into the behaviour of the masonry wall under an out-of-plane load. The initial stiffness of the wall can be obtained by dividing the area load by the mid-span displacement. A higher initial stiffness shows a stronger resistance against out-of-plane deformation. Table 5.3 notes the initial stiffness of all bond patterns part of this study and figure 5.8 plots the initial stiffness to the out-of-plane bending capacity. All single wythe bond patterns are grouped, while the double wythe bond patterns have a similar initial stiffness but a relatively more spread out out-of-plane bending capacity. The lowest initial stiffness observed is from the half Flemish bond, which has the highest single wythe bending capacity. If any correlation would be present, the highest initial stiffness would correspond to the lowest out-of-plane bending capacity or reversely to the highest out-of-plane bending capacity. This is however not the case. The highest initial stiffness for the single wythe bond patterns is the stretcher bond which has the second highest out-of-plane bending capacity. Another similar case can be observed for the double wythe bond patterns. The English bond has the lowest initial stiffness of the double wythe bond patterns and also the lowest out-of-plane bending

capacity of the double wythe bond patterns. Contrarily, the chain bond has the highest initial stiffness but its out-of-plane bending capacity sits between the other double wythe bond patterns. Additionally, the half Flemish bond has the highest out-of-plane bending capacity of the single wythe bond patterns but the lowest initial stiffness. There is thus no correlation between the out-of-plane bending capacity and the initial stiffness due to the bond patterns. The wythe of the masonry wall does influence the initial stiffness as shown in the graph.

The slope of the crack pattern can relate to the out-of-plane bending capacity. The slope of the crack pattern is the angle shown in figure 5.9. The crack patterns of the bond patterns are shown in figure 5.3 and the slopes are noted for all bond patterns in table 5.3. The slope of the crack pattern of the stack bond could not be determined as no crack pattern has formed. The bond patterns with the highest out-of-plane bending capacity for each wythe are the half Flemish bond and the Flemish bond. These bond patterns also have a shallow slope of the crack pattern with 27.4° and 31.3°. These are not the only bond patterns with a shallow slope, the chain bond has a slope of 32.8°. The chain bond does have a lower out-of-plane bending capacity though. The steepest slope of 48.3° is observed with the English bond which also has the lowest double wythe out-of-plane bending capacity. The stretcher bond and the quarter bat bond have a slope in between these extremes and are also in the middle of the spread of the out-of-plane bending capacities of the single wythe bond patterns. There is one exception in the comparison between the slope of the crack pattern and out-of-plane bending capacity: the lateral bond. The lateral bond is the only asymmetric bond pattern and also the only bond pattern with an asymmetric crack pattern. Therefore, there are two slopes noted in the table, a steep slope of 51.3° and a shallow slope of 27.4°. This contradiction coincides with the lowest out-of-plane bending capacity of all bond patterns. The shallower the slope of the crack pattern is, higher the out-of-plane bending capacity.

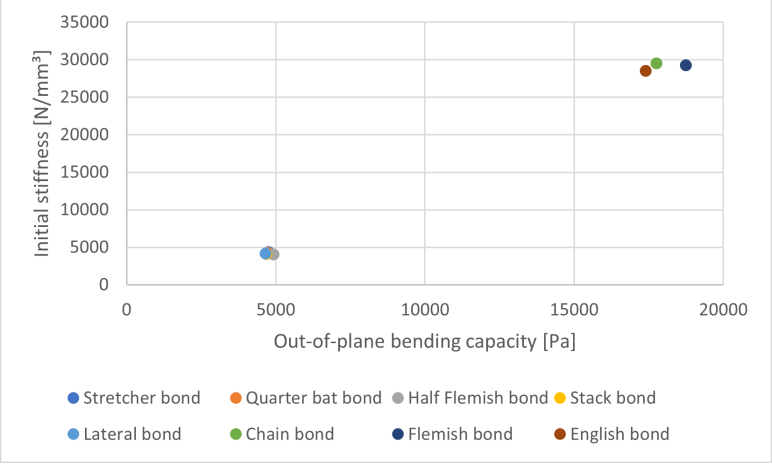

Figure 5.8: The stiffness of the masonry wall compared to the two-way bending capacity

Table 5.3: Initial stiffness and slope of the crack pattern for all bond patterns, the slope of the crack pattern is shown in figure 5.9

Bond pattern	Initial stiffness	Slope of the crack pattern
Stretcher bond	4 356.8 N/mm^3	41.1°
Lateral bond	4 196.0 N/mm^3	27.4°/ 51.3°
Quarter bat bond	4 224.7 N/mm^3	41.1°
Half Flemish bond	4 020.0 N/mm^3	27.4°
Stack bond	4 096.9 N/mm^3	-
Chain bond	29 496 N/mm^3	32.8°
English bond	28 542 N/mm^3	48.3°
Flemish bond	29 294 N/mm^3	31.3°

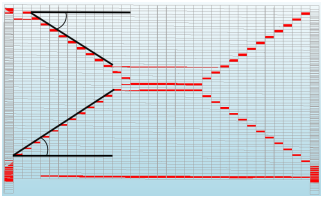

Figure 5.9: The angle used for determining the slope of the crack pattern

5.4. CONCLUDING REMARKS

The highest out-of-plane bending capacity of the single wythe bond patterns is the half Flemish bond with 4.92 kPa. The bond pattern with the lowest bending capacity is surprisingly the lateral bond with 4.65 kPa. This means that the spread of the two-way out-of-plane bending capacities of the single wythe bond patterns is within 0.27 kPa, or 5.4%. The fact that the stack bond does not have the lowest bending capacity can be explained by an equality of the material properties and thickness of the head joint compared to the bed and collar joints. A weaker head joint would probably reduce the out-of-plane bending capacity of the stack bond significantly.
The double wythe bond pattern with the highest out-of-plane bending capacity is also the Flemish bond with 18.7 kPa. In the case of the double wythe are the two-way out-of-plane bending capacities spread further apart, 1.3 kPa or 7.2%. The doubling and interlocking resulted in a bending capacity increase of 280%.
The bond patterns can also be compared by the initial stiffness and the slope of the crack pattern. However, the initial stiffnesses of the masonry walls are separated by wythe, not the out-of-plane bending capacity. The initial stiffness does not influence the out-of-plane bending capacity. The slope of the crack patterns can also be determined for all bond patterns, except for the stack bond which developed no crack pattern. The slope of the crack pattern is the angle between the diagonal of the crack pattern and the horizontal. The bond pattern with the highest out-of-plane bending capacity (half Flemish bond and Flemish bond) both have shallow slopes in their crack pattern. The steepest slope is from the English bond, which has the lowest out-of-plane bending capacity of the double wythe bond patterns. The only exception is the lateral bond, as it is the only bond pattern which is asymmetric. The crack pattern of the lateral bond is not a smooth cross-yielding pattern. The left side of the crack pattern has the steepest slope observed while the right side has an equal slope to the half Flemish bond. This contradiction coincides with the lowest out-of-plane bending capacity of all bond patterns. A shallow slope for the crack pattern relates to a high out-of-plane bending capacity.

6

Conclusion and Recommendations

6.1. Conclusion

The main type of failure for unreinforced brick masonry wall under lateral load is out-of-plane failure. A masonry wall can resist the lateral load by the mechanism of one-way bending when supported only at the top and bottom edge, and two-way bending when supported on 3 or more edges. In the past, the effect of openings in the wall and the aspect ratio of the wall on the two-way out-of-plane bending capacity has been studied. On the contrary, the effect of the bond pattern and the thickness of the wall has not been studied. This thesis has analysed the two-way out-of-plane bending capacity for five single wythe bond patterns and three double wythe bond patterns. The two-way bending capacity was determined using a numerical model adapted from Chang et al. [1, 2]. This model can accurately estimate the initial stiffness and out-of-plane bending capacity, post-peak the model is less accurate. The numerical model has been calibrated and validated by Chang et al. [1, 2] with the data from Griffith et al. [3].

The numerical model is a Finite Element Method (FEM) model and uses a Block-based model (BBM). A Block-based model is necessary to implement the bond patterns as this is not possible in a continuum homogeneous model (CHM). The assembled model consists of solid elements for the bricks and zero-thickness interfaces for the mortar joints. The mortar joints are modelled as zero-thickness elements, so the bricks are expanded to maintain the overall geometry. For the bricks, a rotating smeared cracking model considering an exponential tensile softening and an elastic response in compression was considered. For the mortar joints, the combined cracking-crushing-shear interface model was considered with an exponential softening in tension and shear and a parabolic curve in compression. It is assumed that the material properties of the mortar in the bed joints are the same as the one of the head and collar joints. The masonry wall was first subjected to self-weight and a vertical pre-compression of 0.1 MPa. Afterwards, a monotonic out-of-plane pressure placed on the face of the masonry wall is applied. The

double wythe masonry wall has been assembled by adding an outer shell to the single wythe wall and by decreasing the pre-compression to 0.0478 MPa to maintain the same vertical load. The out-of-plane bending capacity is influenced by the pre-compression, a higher pre-compression results in a higher out-of-plane bending capacity [3]. The numerical model takes both physical and geometrical nonlinearity into account.

One modification to the original model from Chang et al. [1, 2] is a change in mesh size of the bricks. Three mesh sizes have been compared, halfbrick (Hbrick), quarterbrick (Qbrick) and octogonalbrick (Obrick). In the original model of Chang, the face of the brick was divided over its length into two parts called a halfbrick (Hbrick). The stretcher bond can be implemented in a mesh size this large, however other bond patterns require a division of the face over its length into 4 parts, a quarterbrick (Qbrick). An even smaller mesh size which maintains the aspect ratio of the face of the Hbrick by halving the Qbrick along its height is also tested, an octogonalbrick (Obrick). The height of mesh of the Hbrick and Qbrick is equal to the height of the brick. In all three mesh sizes is the depth of the brick divided in three parts, this has been verified by Chang et al. [1]. The Qbrick and Obrick were compared to the Hbrick and showed no difference in initial stiffness, out-of-plane bending capacity and post-peak response. The Obrick consisted of significantly more nodes and therefore reduced the length of the analysis due to convergence issues. The analysis of the Obrick stopped at a mid-span displacement of 3 mm while the Hbrick and Qbrick reached mid-span displacements of 18.5 and 15.5 mm, respectively. The shorter analysis also resulted in an undeveloped crack pattern. The calculation time of the Obrick analysis also increased significantly. The Qbrick can be used instead of the Hbrick.

The numerical model uses a smeared cracking model within the bricks. This results in an absence of cracks through the brick as the crack is smeared out over the element. The crack pattern of the experiments by Griffith et al. [3] and Padalu et al. [4] show that vertical cracks do propagate through the bricks. To attempt to achieve a similar crack pattern a comparison with a discrete cracking model was evaluated. The discrete cracking model requires the user to choose the location of the cracks. These can accurately be assumed, namely in the middle of the brick in line with the joints in the courses above and below. This cracking model is only for the bricks, the interface elements for the mortar joints still have their original yield function. These cracking models have been compared in a masonry wall with the stretcher bond and they have similar two-way out-of-plane bending capacities and identical initial stiffnesses. There is a difference in the load-displacement curve post-peak as the smeared cracking model plateaus on a lower load level. Eventually, the discrete cracking model was not used as the out-of-plane bending capacity was not impacted, while convergence issues arose. The discrete model struggled or even failed to converge within reasonable computation time. During the numerical analysis no cracks were observed within the brick. Bricks with weaker material properties might introduce cracks within the brick and require the discrete cracking model to be simulated accurately.

The effect of the length of the return wall was also studied. In the experiment by Griffith et al. [3] a return wall of 480 mm was used and the ends of the return walls were clamped by C-shaped channels. These clamps prevent any horizontal translations and rotations

in the horizontal plane. The clamps are represented by tyings in the numerical model and the tyings are straight lines stretching from the bottom course to the top course situated at the edges of the end of the return walls. The bottom of the line is connected to the mortar joint between the bottom course and the vertical support. The tyings equalise both horizontal translations for all nodes on the line and as such the end of the return wall moves as one piece. All horizontal movement is prevented as the tyings are connected to the support. The location of the tyings ensures no rotation. To determine the effect of these tyings, they are removed and then the length of the return wall has been parameterised. Especially the shortening of the return wall resulted in weakening the boundary conditions and introduced one-way out-of-plane bending. The lack of a return wall resulted in only one-way out-of-plane bending and the increase to a length of 480 mm shows the transition to two-way out-of-plane bending. Return walls longer than 480 mm were only two-way out-of-plane bending. The masonry wall with the tyings also shows only two-way bending and the effect of the tyings is a spread of only 7.5% of the out-of-plane bending capacity to return walls of lengths of 480 mm and longer. This is a small difference but will probably remain. As the difference in out-of-plane bending capacity is small, it can be determined that the tyings are an appropriate and acceptable simplification to simulate a clamped return wall. The assembly of the double wythe walls included adding additional tyings to maintain this clamping.

A verification of the assumption of compressive behaviour of the bricks is also performed. The bricks have a characteristic compressive resistance while the numerical model assumes that the compressive behaviour is elastic. This means that nonlinear effects like crushing are not modelled. The maximum value of the minimum principal stress is determined for the single wythe stretcher bond and double wythe Flemish bond and are 11.35 MPa and 15.18 MPa, respectively. These are below the compressive resistance of 16 MPa of the bricks and the material properties are thus not exceeded. These peaks of compressive stresses occur on the edge of a brick, half a brick from the return wall. This is the location of the greatest global rotation of the masonry wall. The compressive stress is not a problem in this study; however, it will become a problem if weaker bricks are used or an additional wythe is added.

The effect of the bond patterns on the two-way out-of-plane bending capacity is negligible. The five single wythe bond patterns are spread within 5.4% of the half Flemish bond and the double wythe bond patterns are spread within 7.2% of the Flemish bond. The half Flemish bond and Flemish bond have the highest out-of-plane bending capacity of their number of wythe with 4.9 kPa and 18.7 kPa, respectively. The double wythe bond patterns have an out-of-plane bending capacity which is 280% higher than the single wythe bond patterns. The differences between bond patterns with equal wythe can be easily overcome by using other relative material properties between the bricks and mortar. As the tensile, compressive and shear behaviour of the bricks and mortar influences the out-of-plane capacity. In this case, stronger material properties of the mortar joints would increase the out-of-plane bending capacity.

The overall type of failure is very similar as all bond patterns produced a cross-yielding crack pattern. The only exception is the stack bond, the crack pattern of the stack bond consists of a couple horizontal and vertical cracks, only both horizontal cracks are in

similar locations compared to the crack patterns of the other bond patterns. The slope of the crack pattern (angle of the diagonal of the crack pattern to the horizontal) does relate to the out-of-plane bending capacity. Symmetric bond patterns (excluding the stack bond) have the following relationship: the shallower the slope, the higher the out-of-plane bending capacity. The initial stiffness of the masonry wall does not impact the two-way out-of-plane bending capacity.

6.2. RECOMMENDATIONS

To further confirm these findings, research is needed in relation to different masonry types, considering relative properties between bricks and mortar joints, different properties between bed, head and collar joints, and spatial variability of properties. In this study, no cracks were observed throughout the bricks and neither compressive failure of the bricks is observed but it might occur when bricks with weaker material properties are used. In this study, the same mechanical properties were assigned to all the joints; however, in practice it is often observed that head and collar joints are less filled than bed joints, consequently having lower tensile and shear properties. This aspect may influence the crack propagation with consequences on the two-way out-of-plane bending capacity. This effect can be especially relevant for the stack bond. Additionally, the spatial variability might offer additional paths for the crack to propagate through. The cuts into the bricks to obtain the shorter length bricks are assumed to be perfect.

REFERENCES

[1] L. Z. Chang, J. Rots, and R. Esposito. “Influence of aspect ratio and pre-compression on force capacity of unreinforced masonry walls in out-of-plane bending”. In: *Elsevier* (2021).

[2] L. Z. Chang, J. Rots, and R. Esposito. “Influence of openings on two-way bending capacity of unreinforced masonry walls”. In: *Elsevier* (2022).

[3] M. C. Griffith and J. Vaculik. “Out-of-plane flexural strength of unreinforced clay brick masonry walls”. In: *TMS Journal* 25 (2007), pp. 53–68.

[4] P. K. V. R. Padalu, Y. Singh, and S. Das. “Cyclic two-way out-of-plane testing of unreinforced masonry walls retrofitted using composite materials”. In: *Elsevier* (2019).

[5] L. Z. Chang, F. Messali, and R. Esposito. “Capacity of unreinforced masonry walls in out-of-plane two-way bending: A review of analytical formualtions”. In: *Elsevier* (2020).

[6] H. W. H. West, H. R. Hodgkinson, and B.A. Haseltine. “The resistance of brickwork to lateral loading, Part 1: experimental methods and results of tests on small specimens and full sized walls”. In: *Struct. Eng.* 55 (1977), pp. 411–421.

[7] B. Chen. “Masonry Walls with Openings under Out-Of-Plane Loading”. Master Thesis. McMaster University, 2002.

[8] V. L. Chong. “The Behaviour of Laterally Loaded Masonry Panels with Opening”. PhD thesis. Plymouth, UK: University of Plymouth, 1993.

[9] H. Derakhshan et al. “Out-of-plane strength of existing two-way spanning solid and cavity unreinforced masonry walls”. In: *Structures 2018* 13 (2018), pp. 88–101.

[10] F. Graziotti et al. “Experimental response of URM single leaf and cavity walls in out-of-plane two-way bending generated by seismic excitation”. In: *Construct. Build. Mater.* 195 (2019), pp. 650–670.

[11] F. Messali et al. “Large-scale testing program for the seismic characterization of Dutch masonry walls”. In: Santiago, Chile: 16WCEE, 2017.

[12] R. van der Pluijm. “Report TUE-BCO_9903: Test on laterally loaded clay brick panels”. In: *Eindhoven university of Technology* (1999).

[13] R. van der Pluijm. “2001-CON-BM-R5015: Laterally Loaded Masonry Panels made with Thin Layer Mortar”. In: *TNO* (2001).

[14] G. Ravenshorst and F. Messali. “Out-Of-Plane Tests on Replicated Masonry Walls. Report No. C31B60-6”. In: *Delft University of Technology* (2016).

[15] C. Southcombe and A. Tapp. “Investigation of laterally loaded brickwork panels with openings”. In: *Masonry* 2 (1988), pp. 112–114.

[16] J. Vaculik. “Unreinforced Masonry Walls Subjected to Out-Of-Plane Seismic Actions”. PhD thesis. Adelaide, Australia: University of Adelaide, 2012.

[17] M. C. Griffith and J. Vaculik. “Out-of-plane shaketable testing of unreinforced masonry walls in two-way bending”. In: *Bulletin of Earthquake Engineering* 16 (2017), pp. 2839–2876.

[18] R. C. de Vekey et al. “The resistance of masonry to lateral loading, Part 3: research results on autoclaved aerated concrete blockwork”. In: *Struct. Eng.* 64 (1986), pp. 332–340.

[19] A. M. D’Altri et al. “Modeling Strategies of the Computational Analysis of Unreinforced Masonry Structures: Review and Classification”. In: *Springer* (2019).

[20] D. Ferreira and J. Manie. *Diana Documentation Release 10.5*. 2022. URL: https://manuals.dianafea.com/d105/Diana.html.

List of Figures

List of Tables

A

CONVERGENCE BEHAVIOUR

The iterations per load step in the analysis are shown for all the bond patterns and additional checks part of chapter 4. For all numerical models the maximum iterations per load step is 500, the only exception is the discrete cracking model (figure A.1a), to attempt to reach more convergence has the maximum amount of iterations been upped to 1000. This did not give better results.

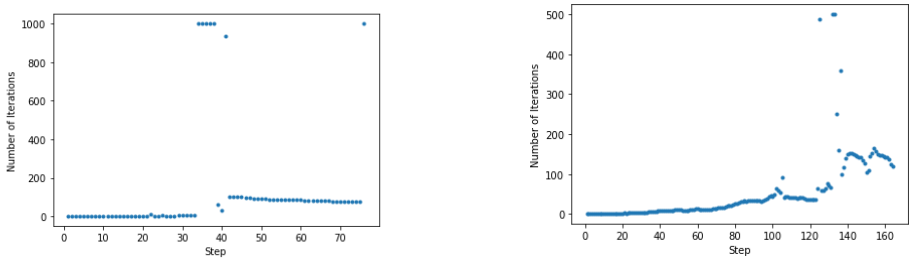

(a) Discrete cracking model

(b) Meshsize; octagonalbrick (Obrick)

Figure A.1: Iterations per load step, discrete cracking model and Obrick

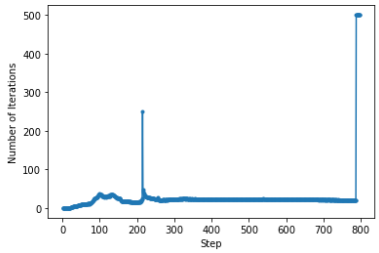

(a) Stretcher bond

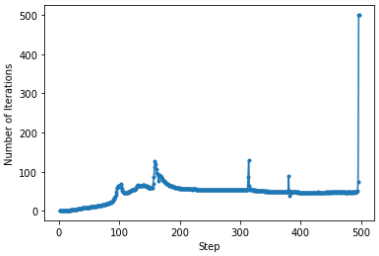

(b) Lateral bond

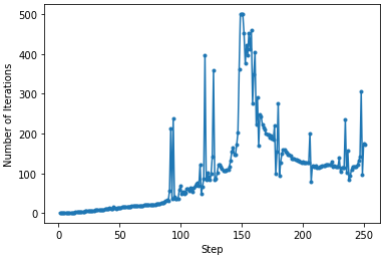

(c) Quarter bat bond

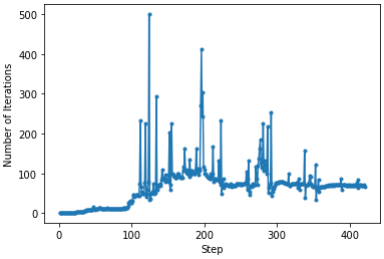

(d) Half Flemish bond

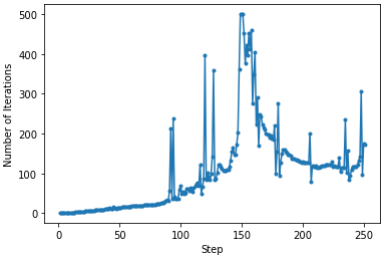

(e) Stack bond

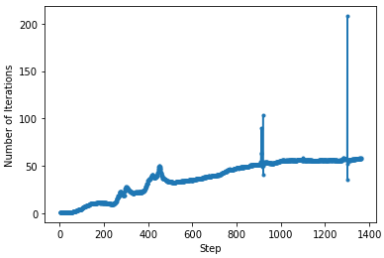

(f) Chain bond

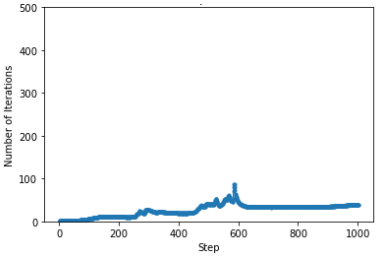

(g) English bond, manually stopped at 1000 steps

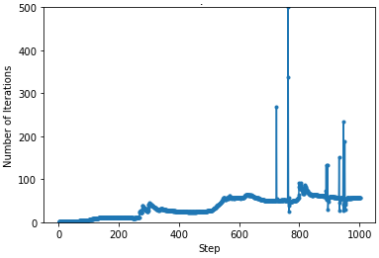

(h) Flemish bond, manually stopped at 1000 steps

Figure A.2: Iterations per load step, all bond patterns

B

GRAPHS LENGTH OF RETURN WALL

The graph combines all load-displacement curves for the 10 different lengths of the return wall and the clamped situation. After 4 halfbricks (Hbricks) the results converge to the same displacement. The 1, 2 and 3 Hbricks have a significantly weaker out-of-plane two-way bending capacity compared to the longer lengths. The clamped situation has the highest out-of-plane bending capacity.

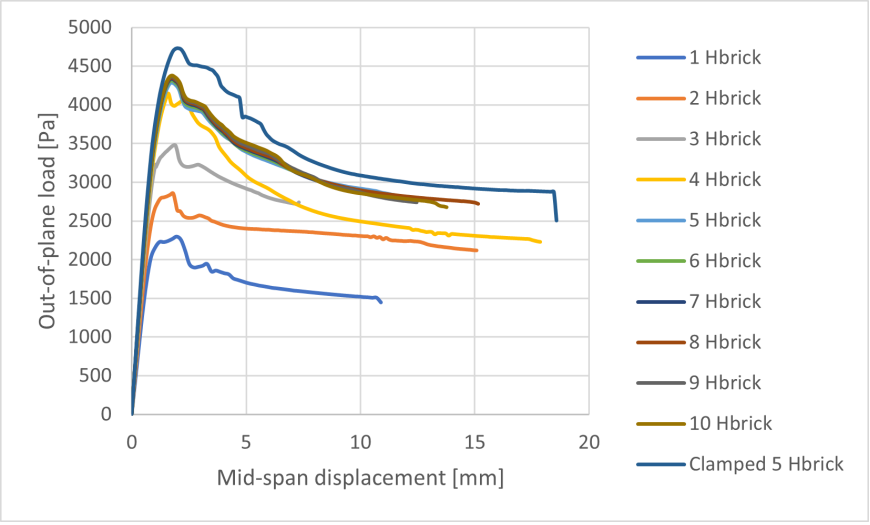

Figure B.1: The load-displacement curve of all lengths of the return wall